Yin-Yang grid in Numerical Relativity

Master's thesis

Wasilij Barsukow

2014

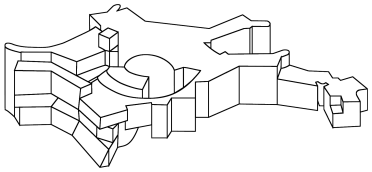

Version: September 30, 2014

Abstract

The presence of coordinate singularities makes the implementation of hydrodynamics and relativity on spherical polar grids a challenging task. This thesis presents an implementation of the so-called Yin-Yang grid into a numerical relativity code that uses spherical polar coordinates. The grid allows one to remove the polar singularities by considering for every 2-sphere two coordinate patches. It also has the advantage of reducing the severeness of the Courant condition, which is normally very restrictive in spherical polar coordinates. An overview of numerical relativity in the BSSN formulation and of relativistic hydrodynamics in the context of spherical polar grids precedes a discussion of numerical algorithms and a detailed description of the geometry and implementation of the Yin-Yang grid. The code was tested on both vacuum and non-vacuum spacetimes and is found to perform stably on the implemented grid.

Zusammenfassung

Koordinatensingularitäten erschweren die Implementierung der Methoden numerischer Hydrodynamik und Relativitätstheorie auf sphärischen polaren Gittern, für astrophysikalische Anwendungen ist die Wahl dieser Koordinaten aber attraktiv. In dieser Masterarbeit wird zum ersten Mal das sogenannte Yin-Yang-Gitter für die numerische Integration der Einstein-Gleichungen der Allgemeinen Relativitätstheorie verwendet. Dieses überdeckt jede 2-Sphäre mit zwei Karten, von denen jede sphärische Polarkoordinaten nutzt, die Achsen der Koordinatensysteme aber zueinander orthogonal sind. Neben der Entfernung der Polregion wird die in gewöhnlichen Polarkoordinaten sehr restriktive Courant-Bedingung gemildert. Die Gleichungen (in der auf einer Hintergrundmetrik basierenden BSSN-Form) werden mit einer teilweise impliziten Runge-Kutta Methode integriert. Die Implementierung der relativistischen Hydrodynamik nutzt konservative Methoden mit hoher Auflösung von Schockfronten. Die Stabilität des Gitters wird an Vakuum und nicht-Vakuum Raumzeiten demonstriert.

Contents

Acknowledgments

My stay at the Max-Planck Institute for Astrophysics in Garching would not have been possible without the warm welcome by Ewald Müller, he and Pedro Montero have supported me at all stages of the work. I would like to express my gratitude to both of them. Thomas W. Baumgarte and Matthias Bartelmann I am equally obliged to thank for their support and many fruitful discussions. Numerous people at the MPA have given me new insights into their work, were an inspiration for me and a pleasure to work with. I particularly enjoyed discussions with Hannes Grimm-Strele, Maxime Viallet, Annop Wongwathanarat and Philipp Edelmann and I am obliged to thank them for enduring and answering my questions and giving valuable ideas.

1 Introduction

General relativity comes into play in a variety of astrophysical situations, mostly involving compact objects and black holes. Gravitational wave astronomy is expected to provide major advances in the study of the internal structure of many objects and tests of general relativity in the strong field regime. The equations of general relativity (found nearly hundred years ago) have so far not allowed for exact solutions but in highly symmetric situations or were solved in only an approximate manner. Putting all ingredients together necessary to model a true astrophysical object to some detail is only possible in a simulation, thus justifying the quest for reliable ways to solve the Einstein equations numerically.

Several methods for doing this have been proposed (e.g. [Ise07], [WMM96]; [Pre05]; [BLPŽ03]; [BGGN04]; [BS98]; [Win05]). The most successful ones are based on the $3+1$ decomposition of spacetime, invented in the mathematical literature in the 1920s. As the Einstein equations do not develop discontinuities, they can be discretized with finite differencing. In non-vacuum spacetimes the equations for the spacetime evolution have to be augmented by those of relativistic hydrodynamics, for which the method of choice are grid based shock-capturing methods employing finite volume or finite difference approximations.

Many astrophysical problems seem to be well captured in spherical polar coordinates. To implement a computational grid induced by spherical polar coordinates one needs to circumvent additional difficulties due to the presence of coordinate singularities on the polar axis and at the origin. Although possible ([BMCCM13]), spherical polar codes suffer from a rather restrictive Courant condition and accumulate errors in the vicinity of the axis. No relevant practical situation is of course perfectly spherically symmetric, and thus full three-dimensional spherical polar grids may be seen as just a first stage towards more complicated grid geometries, as for example have been studied recently in [GSKM14] for hydrodynamics. Another approach to treat problems arising from coordinate singularities is to switch to other grids, in the spirit of minimal change. This has been done in hydrodynamics (e.g. [GR62]; [Phi59], [Sad72], [RIP96]; [SAM68], [Wil68], [RRH$^+$02]; [CDH$^+$08]) and one such approach is particularly suitable: the *Yin-Yang grid* [KS04]. Its implementation is facilitated by the fact that it involves two pieces of usual spherical polar coordinates. In [WHM10] this grid has been successfully implemented for Newtonian hydrodynamics. This thesis presents the first implementation of such a grid for the solution of the Einstein equations and general relativistic hydrodynamics.

Section 2 gives a brief overview of the $3+1$ formulation of the Einstein equations, followed by the BSSN formulation in a form suitable for implementation on a non-Cartesian grid, and a short introduction into relativistic hydrodynamics. Section 3 presents basic ideas on finite difference and finite volume schemes. Section 4 describes the challenges in spherical polar coordinates as well as the geometry and the implementation of a Yin-Yang grid. In Section 5 tests of both vacuum and non-vacuum spacetime evolutions follow.

Conventions

- The metric signature is $(-,+,+,+)$. Summation over upper and lower indices is always assumed, latin indices run over 1, 2, 3, greek ones over 0, 1, 2, 3.
- The units are such that $G = c = M_\odot = \pi = 1$.
- $\mathbb{N} = \{1, 2, \ldots\}$, $\mathbb{N}_0$ denotes $\mathbb{N} \cup \{0\}$.
- $A := B$ denotes the definition of A as a new name for expression B. $A \equiv B$ means identity between expression A and B for any parameter values involved.
- *smooth* means belonging to $C^\infty = \bigcap_{k\in\mathbb{N}_0} C^k$, where the differentiability class C^k contains functions, whose first k derivatives exist and are continuous, with $k = 0$ referring to the function itself.
- Vectors noted as columns or rows and analogously matrices are given with respect to a Cartesian basis, if not stated differently.
- $\mathfrak{id}$ denotes the identity map, with the space involved suppressed ($\mathbb{R}^3$ by default).
- Angular coordinates, if not stated differently, are always given in the form and order (ϑ, φ). Similarly numbers of grid cells are denoted in the order $N_r \times N_\vartheta \times N_\varphi$.
- The floor function $\lfloor x \rfloor$, $x \in \mathbb{R}$ denotes the largest integer less or equal x. The expression $n \equiv r \mod b$ with $n, r \in \mathbb{N}_0$, $b \in \mathbb{N}$ means that $n = k \cdot b + r$ for some $k \in \mathbb{N}_0$. The same equation can be used with $n, r, k \in \mathbb{R}$, $b \in \mathbb{R}\backslash\{0\}$.

2 $3+1$ formulation of the Einstein equations

> A stupid man's report of what a clever man says
> is never accurate because he unconsciously translates
> what he hears into something that he can understand.
> Betrand Russell, *History of Western Philosophy*

2.1 Overview

The equations of general relativity are about the *spacetime*, a 4-dimensional manifold with a special 2-tensor, the *metric*. They express the dependence of the metric on the energy content. These are partial differential equations of second order and have as such attracted the attention of the mathematical community, questioning the existence and uniqueness of solutions up to coordinate transformations. The answers have been given by Yvonne Choquet-Bruhat [FB52] in the 1950s, with important contributions from her doctoral father and grandfather, Lichnerowicz and Darmois. The framework of Choquet-Bruhat's work was the Cauchy problem, i.e. initial data given on a spacelike hypersurface.

The $3+1$ formulation of general relativity is based on the related concept of a *foliation* of spacetime by spacelike hypersurfaces. All quantities appearing in the Einstein equations are projected on such a surface and on the normal, respectively, thus finally obtaining the $3+1$ decomposition of the Einstein and of the energy-momentum-tensor. The equations are then expressed as a family of *evolution equations* from one hypersurface to another and a family of *constraints*. This splitting is often compared to the Maxwell equations, two of which involve time derivatives and two do not.

One feature of relativity is that an equation for coordinates is not provided. It is in principle not needed, as they could be fixed once for all, but it turns out to be useful to evolve them together with the other spacetime quantities. This is connected to a second particularity of relativity: the appearance of singularities, both coordinate and physical ones. Coordinate prescriptions that avoid the formation of coordinate singularities are very much in use.

This chapter is largely influenced by the enlightening book by Gourgoulhon ([Gou12]). However some of the notation is different. $v^\flat$ and $\omega^\sharp$ are considered better notations for the metric duals of a vector v and a 1-form ω, than arrows. Boldface for vectors and tensors, when written down in a coordinate-free manner is considered unnecessary, to define the trace of a mixed 2-tensor A the notation $\operatorname{tr} A := A^\mu{}_\mu$ is adapted. As the quantities on a hypersurface will be most relevant, the four-dimensional counterparts are equipped with a leading superscript 4, i.e. the four-dimensional Ricci scalar will be denoted as ${}^4R$, this time in agreement with the practice in the book.

2.2 Differential geometry on a hypersurface

Call $T_p(M)$ the tangent space at p of a spacetime M, which is a manifold equipped with a metric ${}^4g : T_p(M) \times T_p(M) \to \mathbb{R}$. Given a hypersurface Σ as an embedding $\Phi(\hat{\Sigma})$ of a 3-dimensional manifold $\hat{\Sigma}$, one can define the pullback Φ^* and use it to define the induced metric $\gamma : T_p(\Sigma) \times T_p(\Sigma) \to \mathbb{R}$. Helpfully, it turns out that when the hypersurface is defined as one of constant time x^0, then for the remaining coordinates x^1, x^2, x^3 one finds ${}^4g_{ij} = \gamma_{ij}$.

As on any other manifold, quantities like the Riemann and Ricci tensors and scalar (Riem and Ric and R whenever not involving coordinates, otherwise all of them denoted by R, distinguishable by the number of indices) are defined. The spacetime connection is denoted by ∇ as usual, the connection with respect to the induced metric by D.

Having an embedding allows one to define additional quantities, as the notion of a normal vector is clear. Given a hypersurface Σ defined as a level surface of t, the gradient ∇t is normal to the hypersurface, i.e. taking every vector tangent to Σ to zero. The normalized metric dual n of ∇t (if Σ is not null) is chosen to be

$$n \cdot n = \begin{cases} -1 & \Sigma \text{ spacelike} \\ 1 & \Sigma \text{ timelike} \end{cases}$$

n is called a *normal vector* (field).

Given a normal n and a tangent vector v the *Weingarten map* $\chi : T_p(\Sigma) \to T_p(\Sigma)$ measures the change of the normal in a given direction along Σ. This change will not be zero, if the hypersurface is extrinsically curved and is defined as $\nabla_v n$. Taking n as a second parameter one obtains the *second fundamental form* of the hypersurface, or its *extrinsic curvature tensor* K:

$$\begin{aligned} K : T_p(\Sigma) \times T_p(\Sigma) &\to \mathbb{R} \\ (u, v) &\mapsto -u \cdot \chi(v) \end{aligned}$$

The Weingarten map is self-adjoint (K is symmetric); its real eigenvalues are called *principal curvatures* and the eigenvectors *principal directions*. The mean curvature is the arithmetic mean of the principal curvatures, i.e. it is equal to $-\frac{1}{3}\operatorname{tr} K$.

2.3 Slicings

The $3 + 1$ formulation of relativity assumes the spacetime to be foliated, or sliced by spacelike hypersurfaces, each labeled by some time coordinate. This setup has been used for long in the context of existence and uniqueness theorems, because it is a natural framework of a Cauchy problem.

A *causal* curve is a curve whose tangent is either timelike or null. A future (past) directed causal curve $\gamma : (a, b) \to M$ is said to be *future (past) inextendible* in M if $\lim_{t \to b^-} \gamma(t)$ does not exist.

A *Cauchy surface* is a spacelike hypersurface, such that each inextendible, causal curve intersects it only once. Clearly, a spacetime with e.g. closed timelike curves does not admit a Cauchy surface.

The existence of Cauchy surfaces is tightly linked to the notion of *global hyperbolicity*. It turns out that in order to admit a Cauchy surface the spacetime has to be globally hyperbolic; the converse is true as well. Global hyperbolicity thus enters into the important statements about the existence and uniqueness of solutions to the Cauchy problem in general relativity. At the same time such a spacetime admits a time function, which can be used to introduce a *slicing* of the spacetime:

A *slicing* of a spacetime is a set of continuously and uniquely parametrized (by $t \in \mathbb{R}$, say) non-intersecting hypersurfaces Σ_t. Furthermore here all Σ_t are assumed spacelike and filling out all of the spacetime. One can view this as a scalar field t on M (with non-vanishing ∇t) such that each hypersurface is a level surface of t. The scalar field is sometimes called a *time function*.

Further discussion of the precise statements can be found in the Appendix (Sec. 7.1).

One introduces a function α as the scaling between n and ∇t:

$$n^\flat = -\alpha \nabla t$$

n is timelike and of unit length; observers that have n as their 4-velocity are called *Eulerian observers*. α, called the *lapse*, links an interval of proper time $\delta\tau$ for such an observer to the corresponding coordinate time interval δt:

$$\delta\tau = \alpha \delta t$$

which justifies the sign convention and the name.

Associated to the normal vector is the *normal evolution vector* $m := \alpha n$. Consider some point on a hypersurface Σ_t. Displacing it along m yields $p' = p + \delta t m$ and the coordinate time associated with this point is

$$t(p') = t(p) + \delta t \langle \nabla t, m \rangle = t(p) + \delta t,$$

i.e. the hypersurfaces are Lie dragged by m.

The coordinate basis vector ∂_t trivially fulfills the same relation $\langle \nabla t, \partial_t \rangle = 1$. However, (see Fig. 1) the orientation of ∂_t depends on the way how the spatial coordinates on each slice vary. If the lines of constant spatial coordinates are orthogonal to the hypersurfaces, then ∂_t and m coincide. The generally not-vanishing difference between them is called the *shift vector* β:

$$\partial_t = m + \beta \tag{1}$$

β is tangential to the hypersurface. As ∂_t need not be associated with someone's 4-velocity, it can actually be spacelike and the shift would become superluminal. This however are just coordinates.

Having a non-vanishing β gives the following expression for the metric:

$${}^4g_{\mu\nu} \mathrm{d}x^\mu \mathrm{d}x^\nu = -\alpha^2 \mathrm{d}t^2 + \gamma_{ij}(\mathrm{d}x^i + \beta^i \mathrm{d}t)(\mathrm{d}x^j + \beta^j \mathrm{d}t)$$

with $\gamma_{ij} = {}^4g_{ij}$, but $\gamma^{ij} \neq {}^4g^{ij}$ in general.

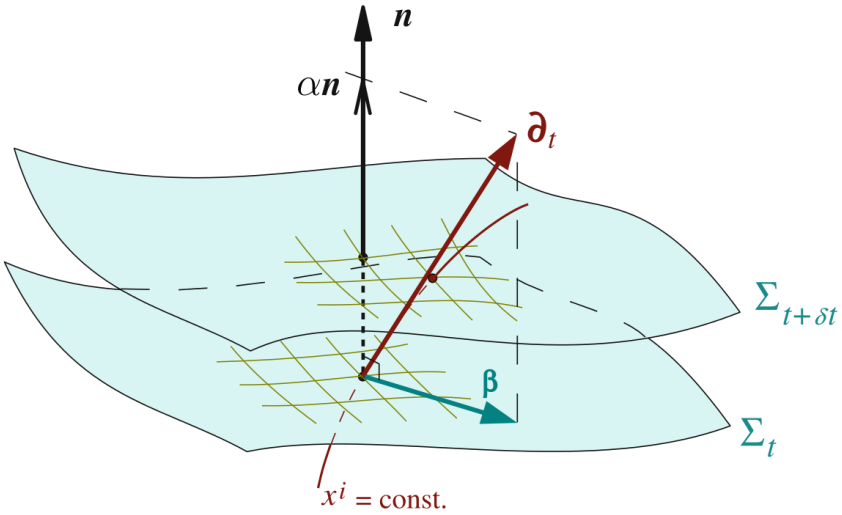

Figure 1: Coordinates (x^i) on the hypersurfaces Σ_t: each line $x^i = \text{const}$ cuts across the foliation and defines the time vector ∂_t and the shift vector β of the spacetime coordinate system (t, x^i). (From [Gou12], Fig. 5.1)

2.4 Einstein equations on a hypersurface

2.4.1 Projection

At each point in a non-null Σ the space of all spacetime vectors can be decomposed orthogonally. Define the projector onto Σ as $P : T_p(M) \to T_p(\Sigma)$, taking a vector v to $v + (n \cdot v)n$, or in components $P^\alpha{}_\beta = \delta^\alpha{}_\beta + n^\alpha n_\beta$. Whereas the embedding of Σ in M induces a mapping from the tangent bundle of Σ to the tangent bundle of M (push-forward), P now does the opposite. This can be used to extend the induced metric $\gamma : T_p(\Sigma) \times T_p(\Sigma) \to \mathbb{R}$ to all of $T_p(M)$, for which the same letter will be kept. One finds then

$$\gamma = {}^4g + n^\flat \otimes n^\flat$$

or in components: $\gamma_{\alpha\beta} = {}^4g_{\alpha\beta} + n_\alpha n_\beta$. Thus the projector P onto Σ is nothing else but the extended induced metric, with one index raised by ${}^4g$. The orthogonal projection map for covariant tensors will be called P^* with

$$\begin{aligned} P^*A : & T_p(M)^k \to \mathbb{R} \\ & (v_1, \dots, v_k) \mapsto A(P(v_1), \dots, P(v_k)) \end{aligned}$$

For example, given a tensor T one has $DT = P^* \nabla T$.

Now via the extension procedure and projections onto n and by P every 4-vector falls apart into a scalar and a 3-vector, every symmetric tensor into a scalar, a vector and a 3-tensor. This is called a $3+1$ *decomposition*. Equation (1) shows already an example: the 4-vector ∂_t is decomposed as $\alpha n + \beta$.

2.4.2 Energy-momentum tensor

The energy density is $E = T(n, n)$. The momentum density is found as $p := -T(P(\cdot), n)$, or in components $p_\alpha = -T_{\mu\nu}\gamma^\mu{}_\alpha n^\nu$ and the matter stress tensor is given as double projection $S = P^*T$, i.e. $S_{\alpha\beta} = T_{\mu\nu}\gamma^\mu{}_\alpha\gamma^\nu{}_\beta$. Combining all of this one finds:

$$T = S + n^\flat \otimes p + p \otimes n^\flat + E n^\flat \otimes n^\flat \tag{2}$$

2.4.3 Gauss relation

Starting from the (four-dimensional) *Ricci identity* connecting the (extended) covariant derivative on Σ and the (extended) Riemann tensor

$$(D_\alpha D_\beta - D_\beta D_\alpha)v^\nu = R^\nu{}_{\mu\alpha\beta}v^\mu$$

one can rephrase it via the four-dimensional spacetime connection ∇ to obtain (after a lot of index gymnastics)

$$(K_{\alpha\mu}K^\gamma{}_\beta - K_{\beta\mu}K^\gamma{}_\alpha)v^\mu + \gamma^\rho{}_\alpha\gamma^\sigma{}_\beta\gamma^\gamma{}_\lambda {}^4R^\lambda{}_{\mu\rho\sigma}v^\mu = R^\gamma{}_{\mu\alpha\beta}v^\mu$$

where the spacetime-Riemann tensor has appeared alongside with the extrinsic curvature of Σ, because of the remarkable relation

$$K = -P^*\nabla n^\flat$$

For its proof the reader is referred to Section 3.4.2 of [Gou12]. The above equation is actually a relation between the tensors already, and carries the name *Gauss relation*:

$$\gamma^\rho{}_\alpha\gamma^\sigma{}_\beta\gamma^\gamma{}_\lambda {}^4R^\lambda{}_{\mu\rho\sigma} = R^\gamma{}_{\mu\alpha\beta} + K_{\beta\mu}K^\gamma{}_\alpha - K_{\alpha\mu}K^\gamma{}_\beta$$

It can be contracted several times to yield

$$\gamma^\mu{}_\alpha\gamma^\nu{}_\beta {}^4R_{\mu\nu} + \gamma_{\alpha\mu}n^\nu\gamma^\rho{}_\beta n^\sigma {}^4R^\mu{}_{\nu\rho\sigma} = R_{\alpha\beta} + \operatorname{tr}K K_{\alpha\beta} - K_{\alpha\mu}K^\mu{}_\beta \tag{3}$$

$${}^4R + 2{}^4R_{\mu\nu}n^\mu n^\nu = R + (\operatorname{tr}K)^2 - K^{ij}K_{ij} \tag{4}$$

which is a generalization of Gauss's *Theorema Egregium* [Gau28].

2.4.4 Codazzi relation

Writing down the Ricci identity for the normal vector

$$(\nabla_\alpha\nabla_\beta - \nabla_\beta\nabla_\alpha)n^\gamma = {}^4R^\gamma{}_{\mu\alpha\beta}n^\mu$$

and projecting it onto Σ one obtains the *Codazzi-Mainardi relation*

$$\gamma^\gamma{}_\rho n^\sigma\gamma^\mu{}_\alpha\gamma^\nu{}_\beta \, {}^4R^\rho{}_{\sigma\mu\nu} = D_\beta K^\gamma{}_\alpha - D_\alpha K^\gamma{}_\beta$$

One contraction yields

$$\gamma^\mu{}_\alpha n^\nu \, {}^4R_{\mu\nu} = D_\alpha \operatorname{tr}K - D_\mu K^\mu{}_\alpha \tag{5}$$

2.4.5 The ADM equations

The Einstein equations without cosmological constant are

$$^4\mathrm{Ric} = 8\pi(^4T - \frac{1}{2}\mathrm{tr}\,^4T g)$$

Using Eqn. (4) one obtains the so-called *Hamiltonian constraint* as a full projection onto the normal:

$$R + (\mathrm{tr}\,K)^2 - K_{ij}K^{ij} = 16\pi E \tag{6}$$

The mixed projection makes the term involving the metric vanish, using the contracted Codazzi relation (5) this gives the *momentum constraint*:

$$D_j K^j{}_i - D_i \mathrm{tr}\,K = 8\pi p_i \tag{7}$$

Using now the full projection onto Σ, i.e. the Gauss relation (3) and a lot of index juggling (see Sec. 4.4 of [Gou12])

$$\mathcal{L}_m K_{ij} = -D_i D_j \alpha + \alpha\left(R_{ij} + \mathrm{tr}\,K K_{ij} - 2K_{ik}K^k{}_j + 4\pi((\mathrm{tr}\,S - E)\gamma_{ij} - 2S_{ij})\right) \tag{8}$$

where the Lie derivative appears as

$$\mathcal{L}_m K_{\alpha\beta} = m^\mu \nabla_\mu K_{\alpha\beta} + K_{\mu\beta}\nabla_\alpha m^\mu + K_{\alpha\mu}\nabla_\beta m^\mu$$

and $m = \alpha n = \partial_t - \beta$. For this reason $\mathcal{L}_m$ is also denoted $\partial_\perp = \partial_t - \mathcal{L}_\beta$.

Calculating $\mathcal{L}_m \gamma_{\alpha\beta}$ one obtains the last needed equation

$$\mathcal{L}_m \gamma_{ij} = -2\alpha K_{ij} \tag{9}$$

System (6), (7), (8) and (9) is referred to as the *ADM equations* [ADM08], although the equations have been known before and are not exactly the same as those derived in the ADM publication, as remarked by [YJ04]. The ADM system splits the Einstein equations into a system very similar to the four Maxwell equations, two of which do not involve time derivatives as well. In order to obtain sensible solutions the constraints have to be fulfilled already at the level of the initial data. In order to verify that the constraints are then also never violated during the evolution, one defines the constraint violations (see e.g. [Fri97])

$$\begin{aligned}\mathcal{E}_0 &:= R + (\mathrm{tr}\,K)^2 - K_{ij}K^{ij} - 16\pi E \\ \mathcal{E}_i &:= D_j K^j{}_i - D_i \mathrm{tr}\,K - 8\pi p_i\end{aligned}$$

and differentiates with respect to t. As the equation thus obtained is of the symbolic form $\partial_\perp \mathcal{E}_\alpha = f(\mathcal{E})_\alpha$ with $f(0) = 0$, a solution is given by $\mathcal{E}_\alpha \equiv 0$, i.e. vanishing for all times. It is of course reassuring that the evolution preserves the constraints.

A nice geometric view is to consider the solution space to the evolution equations, i.e. the space $\mathfrak{S}$ of properly chosen pairs of metrics and extrinsic curvature tensors (in the

vacuum case; matter sources can be added analogously). Equations (8) and (9) determine for each initial data set a curve through this space, parametrized[1] by t (here the existence and uniqueness theorems enter). The constraints $\mathcal{E}_\alpha = 0$ define a subset (submanifold) $\mathfrak{E}$ of this space. The above analysis showed that a solution starting off on $\mathfrak{E}$ will stay on $\mathfrak{E}$ forever. If the constraints are not enforced for the initial data they will however evolve in time; if the evolution equations are not solved precisely (a case relevant in numerics), the solution curve may depart from the constraint-satisfying subset $\mathfrak{E}$.

2.5 BSSN formalism

The exact constraint preservation during the evolution is not expected when it comes to numerical implementations of only the equations (8) and (9) (the evolution system). Slight initial perturbations of the constraints may be amplified during the evolution. If they cannot be controlled the numerical scheme is unstable and cannot be used for practical computations. This turns out to be indeed the case for the ADM equations.

An idea that was already used in Choquet-Bruhat's proof is to transform the equations in such a manner that they become a system for which well-posedness is established. This is only a necessary condition for numerical stability, but it is successfully used as guidance. Different methods have been developed. The one employed here is the BSSN formulation [SN95], [BS98], which will be introduced now briefly.

Its starting point are the ADM equations with a conformal factor and the trace of the curvature evolved separately (York-Lichnerowicz split, [Lic44]). Define

$$\gamma_{ij} =: e^{4\varphi}\tilde{\gamma}_{ij}$$

Conformal decompositions have been used fruitfully in solving the constraint equations. They turn out to be equally relevant in the evolution problem since in [YJ71] it has been pointed out that conformally equivalent 3-metrics lead to equivalent spin-two representations, i.e. ignore all but the two physical degrees of freedom of the gravitational field.

In the original BSSN formulation the determinant $\det\tilde{\gamma}$ was fixed to 1. In order to avoid tensor densities of non-zero weight ([Bro09], [BGGN04]) this condition is replaced by an evolution equation, one of the simplest choices being

$$\partial_t \det\tilde{\gamma} = 0 \tag{10}$$

(called Lagrangian choice in [Bro09]), such that the metric determinant is constant in time and given by its initial value. Thus instead of fixing a numerical condition on the determinant of the conformal metric, one requires it to be equal to the determinant of some other metric, called *background metric* $\hat{\gamma}$. It is then taken as simple as possible, and is in the following assumed to be flat (vanishing curvature, but not necessarily vanishing

[1] Considering a fixed t instead of a fixed initial data set can be made to yield an automorphism of $\mathfrak{S}$, and the time evolution then would correspond to a curve through the (infinite-dimensional) automorphism space.

Christoffel symbols). Eq. (10) means that $\hat{\gamma}$ is glued to the coordinates on the hypersurfaces, which makes the implementation of, e.g., spherical polar coordinates natural (where one takes $\hat{\gamma}$ to be the flat metric in spherical polar coordinates with $\det\hat{\gamma} = r^4\sin^2\vartheta \neq 1$). In any case the conformal factor now becomes a scalar field.

By a trace-free version (TF) of a 2-tensor T_{ij} the expression $T_{ij} - \frac{1}{3}\gamma_{ij}\mathrm{tr}\,T$ is meant. Define

$$A_{ij} := (K_{ij})^{\mathrm{TF}}$$

and

$$A_{ij} =: e^{4\varphi}\tilde{A}_{ij}$$

These definitions in the ADM equations yield

$$\mathcal{L}_m\varphi = -\frac{1}{6}\alpha\mathrm{tr}\,K + \frac{1}{6}\tilde{D}_i\beta^i \tag{11}$$

$$\mathcal{L}_m\mathrm{tr}\,K = -D^iD_i\alpha + \alpha\left(\tilde{A}_{ij}\tilde{A}^{ij} + \frac{1}{3}(\mathrm{tr}\,K)^2\right) + 4\pi\alpha(E + \mathrm{tr}\,S)$$

$$\mathcal{L}_m\tilde{\gamma}_{ij} = -2\alpha\tilde{A}_{ij} - \frac{2}{3}\tilde{D}_k\beta^k\tilde{\gamma}_{ij} \tag{12}$$

$$\mathcal{L}_m\tilde{A}_{ij} = \alpha\mathrm{tr}\,K\tilde{A}_{ij} - 2\alpha\tilde{A}_{ik}\tilde{A}^k{}_j + e^{-4\varphi}\left(-D_iD_j\alpha + \alpha(R_{ij} - 8\pi S_{ij})\right)^{\mathrm{TF}} \tag{13}$$

where $\tilde{\gamma}^{ij}\mathcal{L}_m\tilde{\gamma}_{ij} = \mathcal{L}_m\ln\det\tilde{\gamma}$ has been used and $\tilde{D}_i$ denotes the covariant derivative with respect to the conformally related metric $\tilde{\gamma}$.

The term $D_iD_j\alpha$ can be expressed via $\tilde{D}$:

$$D_iD_j\alpha = \tilde{D}_i\tilde{D}_j\alpha - 4\tilde{D}_{(i}\alpha\tilde{D}_{j)}\varphi + 2\tilde{\gamma}_{ij}\tilde{D}^c\alpha\tilde{D}_c\varphi \tag{14}$$

which gives

$$\mathcal{L}_m\mathrm{tr}\,K = -e^{-4\varphi}\left(\tilde{D}^i\tilde{D}_i\alpha + 2\tilde{D}^i\alpha\tilde{D}_i\varphi\right) + \alpha\left(\tilde{A}_{ij}\tilde{A}^{ij} + \frac{1}{3}(\mathrm{tr}\,K)^2\right) + 4\pi\alpha(E + \mathrm{tr}\,S) \tag{15}$$

The Ricci tensor R_{ij} is a function of the metric γ_{ij}, its inverse, and its first and second derivative. Denoting it as a functional of the metric, one obtains the reformulations

$$\begin{aligned}\mathrm{Ric}[\gamma]_{ij} &= \partial_a\Gamma^a_{ij} - \partial_j\Gamma^a_{ai} + \Gamma^a_{sa}\Gamma^s_{ij} - \Gamma^a_{sj}\Gamma^s_{ai} &(16)\\ &= -\frac{1}{2}\gamma^{am}(\partial_m\partial_a\gamma_{ij} - \partial_i\partial_a\gamma_{mj} - \partial_m\partial_j\gamma_{ia} + \partial_i\partial_j\gamma_{ma}) + \gamma^{am}\left(\Gamma^r_{ia}\Gamma_{rmj} - \Gamma^r_{ij}\Gamma_{rma}\right)\\ &= -\frac{1}{2}\gamma^{am}\partial_m\partial_a\gamma_{ij} + \gamma_{k(i}\partial_{j)}\left(\gamma^{am}\Gamma^k_{am}\right) + \gamma^{am}\Gamma^k_{am}\Gamma_{(ij)k} + \gamma^{am}\left(\Gamma^r_{ia}\Gamma_{rmj} + 2\Gamma^k_{m(i}\Gamma_{j)ka}\right) &(17)\end{aligned}$$

where the second line can be shown by inserting the expressions for Christoffel symbols in terms of the metric derivatives, and the third line by expanding the double derivative and collecting terms. Observe that

$$\gamma^{am}\Gamma^i_{am} \equiv -\partial_m\gamma^{im}$$

Having now a conformally rescaled metric the Ricci tensor can be expressed

$$\mathrm{Ric}[\gamma] = \mathrm{Ric}[e^{4\varphi}\tilde{\gamma}] = \mathrm{Ric}[\tilde{\gamma}] - 2\tilde{D}_i\tilde{D}_j\varphi - 2\tilde{\gamma}_{ij}\tilde{D}^k\tilde{D}_k\varphi + 4(\tilde{D}_i\varphi)(\tilde{D}_j\varphi) - 4\tilde{\gamma}_{ij}(\tilde{D}^k\varphi)(\tilde{D}_k\varphi)$$

Equation (13) then becomes (denoting $\mathrm{Ric}[\tilde{\gamma}]_{ij} =: \tilde{R}_{ij}$ and using (14))

$$\begin{aligned}\mathcal{L}_m\tilde{A}_{ij} =& -\frac{2}{3}\tilde{A}_{ij}\tilde{D}_k\beta^k + \alpha\,\mathrm{tr}\,K\tilde{A}_{ij} - 2\alpha\tilde{A}_{ik}\tilde{A}^k{}_j \\ &+ e^{-4\varphi}\left(-\tilde{D}_i\tilde{D}_j\alpha + 4\tilde{D}_{(i}\alpha\tilde{D}_{j)}\varphi - 2\alpha\tilde{D}_i\tilde{D}_j\varphi + 4\alpha(\tilde{D}_i\varphi)(\tilde{D}_j\varphi) + \alpha(\tilde{R}_{ij} - 8\pi S_{ij})\right)^{\mathrm{TF}}\end{aligned} \tag{18}$$

The principal symbol of (8), which comes from the Ricci tensor (17), is up to factors given by

$$-\frac{1}{2}\tilde{\gamma}^{am}\partial_a\partial_m\tilde{\gamma}_{ij} - \tilde{\gamma}_{k(i}\partial_{j)}\partial_l\tilde{\gamma}^{kl}$$

The first term is a Laplace operator; would it be present alone, it would yield a well understood wave equation. The second term however could be hidden by considering the quantities [BS98] $\tilde{\gamma}^{am}\tilde{\Gamma}^k_{am} \equiv -\partial_m\tilde{\gamma}^{im}$ as independent variables and would seize to be a second derivative, restoring the Laplace operator. Unfortunately these objects would not transform as contravariant vectors. Instead in [Bro09] the quantities

$$\Delta^k_{ij} := \tilde{\Gamma}^k_{ij} - \hat{\Gamma}^k_{ij} \equiv \frac{1}{2}\tilde{\gamma}^{kl}(\hat{D}_i\tilde{\gamma}_{lj} + \hat{D}_j\tilde{\gamma}_{il} - \hat{D}_l\tilde{\gamma}_{ij})$$

are introduced, where $\hat{\Gamma}^k_{ij}$ are the Christoffel symbols of the background metric $\hat{\gamma}$. Δ^i_{jk} are true tensor fields. Replacing $\tilde{\Gamma}^k_{ij}$ in $\mathrm{Ric}[\tilde{\gamma}]$ (from (16)) and using

$$\Delta^k_{ik} \equiv 0$$

and $\mathrm{Ric}[\hat{\gamma}] = 0$ (recall that the background metric is assumed flat) one obtains

$$\begin{aligned}\tilde{R}_{ij} &= \hat{D}_k\Delta^k_{ij} - \Delta^k_{il}\Delta^l_{kj} \\ &= -\frac{1}{2}\tilde{\gamma}^{kl}\hat{D}_k\hat{D}_l\tilde{\gamma}_{ij} + \tilde{\gamma}_{k(i}\hat{D}_{j)}\tilde{\Gamma}^k - \hat{D}_k\tilde{\gamma}_{l(i}\hat{D}_{j)}\tilde{\gamma}^{kl} - \frac{1}{2}\hat{D}_k\tilde{\gamma}^{kl}\hat{D}_l\tilde{\gamma}_{ij} - \Delta^k_{il}\Delta^l_{kj} \\ &= -\frac{1}{2}\tilde{\gamma}^{kl}\hat{D}_k\hat{D}_l\tilde{\gamma}_{ij} + \tilde{\gamma}_{k(i}\hat{D}_{j)}\tilde{\Gamma}^k + \tilde{\Gamma}^k\Delta_{(ij)k} + \tilde{\gamma}^{kl}\left(2\Delta^m_{k(i}\Delta_{j)ml} + \Delta^m_{ik}\Delta_{mjl}\right)\end{aligned} \tag{19}$$

The definition of the additional quantities now involves a contravariant vector:

$$\tilde{\Gamma}^k := -\hat{D}_j\tilde{\gamma}^{ij} \tag{20}$$

The evolution equation for $\tilde{\Gamma}^k$ is found using the evolution equation for $\tilde{\gamma}_{ij}$:

$$\begin{aligned}\mathcal{L}_m\tilde{\Gamma}^i =& \frac{2}{3}\hat{D}_k\beta^k\tilde{\Gamma}^i + \tilde{\gamma}^{jk}\hat{D}_j\hat{D}_k\beta^i + \frac{1}{3}\hat{D}^i\hat{D}_k\beta^k - 2\tilde{A}^{ij}\partial_j\alpha \\ &- 16\pi\alpha\tilde{\gamma}^{ij}p^j + 2\alpha\tilde{A}^{jk}\Delta^i{}_{jk} + 12\alpha\tilde{A}^{ij}\partial_j\varphi - \frac{4}{3}\alpha\tilde{\gamma}^{ij}\partial_j\mathrm{tr}\,K\end{aligned} \tag{21}$$

More details concerning the derivations can be found in Chapters 7, 10 and 11 of [Gou12] as well as in the original publications.

The BSSN system consists of the equations (11), (12), (15), (21), and (18) with (19) for the variables φ, K, $\tilde{\Gamma}^k$, $\tilde{\gamma}_{ij}$ and $\tilde{A}_{ij}$ with

$$\begin{aligned} \det\tilde{\gamma} &= \det\hat{\gamma} \\ \tilde{\gamma}^{ij}\tilde{A}_{ij} &= 0 \end{aligned} \tag{22}$$

and (20) as additional constraints.

2.6 Choice of coordinates

The BSSN system must be supplemented with equations for α and β. In principle the choice $\alpha = 1$, $\beta = 0$ (called *geodesic slicing* and *normal coordinates*) is a valid one. It also belongs to the family of algebraic conditions and thus can be used without solving any equations.

However the disadvantage of $\alpha = 1$ is that if a singularity is present such coordinates typically will hit it and make the code crash (recall that observers reach the Schwarzschild singularity in finite proper time). Thus different conditions on how to relate the different slices have been invented. Here the prescription, called $1 + \log$ [BMSS95],

$$\partial_t\alpha = -2\alpha\,\mathrm{tr}\,K \tag{23}$$

is used. Observe that the β-term that would have been obtained from writing $\mathcal{L}_m\alpha$ on the left hand side has been omitted (both versions are in use in the literature). If $\beta \equiv 0$ then the above equation reduces to $\partial_t\alpha = \partial_t \ln\det\gamma$, hence the name. However, its use does not depend on the value of β. Although singularity avoidance is not guaranteed for the $1 + \log$ slicing (actually the contrary has been shown in [Alc97]), it is used very successfully in simulations.

Given coordinates on some initial slice, β determines how they will look like on all of the foliation. Normal (or Eulerian) coordinates given by $\beta = 0$ are quite useful and also very simple. Another prescription (*Gamma-driver* [ABD$^+$03]), in use here, is

$$\partial_t\beta^i = B^i \tag{24}$$

$$\partial_t B^i = \frac{3}{4}\partial_t\tilde{\Gamma}^i \tag{25}$$

For details on these and other important coordinate evolution schemes the reader is referred to Chapter 10 of [Gou12].

2.7 General relativistic hydrodynamics

The equations to solve are the continuity equation

$$\nabla_\alpha(\rho_0 u^\alpha) = 0$$

and the conservation of the energy-momentum tensor $T^{\alpha\beta} = \rho_0 h u^\alpha u^\beta + {}^4g^{\alpha\beta} P$

$$0 = \nabla_\beta T^{\alpha\beta}$$

with u^α the four-velocity of the fluid, ρ_0 the rest-mass density, $h = 1 + \epsilon + \frac{P}{\rho_0}$ the enthalpy, P the pressure, and ϵ the specific internal energy. The double projection of the energy-momentum tensor ((2)) onto the normal is then given by $E = \rho_0 h W^2 - P$ with $W := -n_a u^a$ being the Lorentz factor between a normal observer and the fluid. For efficient implementation using shock-capturing schemes (see Chapter 3) the equations have to be kept in this form, highlighting conserved quantities and their fluxes. At the same time they have to be expressed in the $3+1$ formalism.

Writing the divergence in the continuity equation as

$$0 = \frac{1}{\sqrt{-\det {}^4g}} \partial_\alpha (\sqrt{-\det {}^4g} \rho_0 u^\alpha) \tag{26}$$

and using $\sqrt{-\det {}^4g} = \alpha e^{6\varphi} \sqrt{\det \tilde{\gamma}}$ one obtains for the spatial part of (26)

$$\begin{aligned} \partial_j (\alpha e^{6\varphi} \sqrt{\det \tilde{\gamma}} \rho_0 u^j) &= \partial_j \left(\sqrt{\det \hat{\gamma}} \alpha e^{6\varphi} \sqrt{\frac{\det \tilde{\gamma}}{\det \hat{\gamma}}} \rho_0 u^j \right) \\ &= \sqrt{\hat{\gamma}} \hat{D}_j \left(\alpha e^{6\varphi} \sqrt{\frac{\det \tilde{\gamma}}{\det \hat{\gamma}}} \rho_0 u^j \right) \end{aligned}$$

and for the full continuity equation

$$0 = \partial_t \left(e^{6\varphi} \sqrt{\frac{\det \tilde{\gamma}}{\det \hat{\gamma}}} d \right) + \hat{D}_j (f_d)^j = \partial_t \left(e^{6\varphi} \sqrt{\frac{\det \tilde{\gamma}}{\det \hat{\gamma}}} d \right) + \partial_j (f_d)^j + (f_d)^j \hat{\Gamma}^k_{jk}$$

with

$$\begin{aligned} d &:= W \rho_0 \qquad \text{density seen by normal observer} \\ (f_d)^j &:= \alpha e^{6\varphi} \sqrt{\frac{\det \tilde{\gamma}}{\det \hat{\gamma}}} d \left(v^i - \frac{\beta^i}{\alpha} \right) \\ v^a &:= \gamma^a{}_b \left(\frac{u^b}{W} + \frac{\beta^b}{\alpha} \right) \qquad \text{fluid velocity for normal observer} \end{aligned}$$

The background metric $\hat{\gamma}$ thus introduced in [MBM14] allows one to write all quantities as tensors. The continuity equation is expressed in what is called conservation form (see Sec. 3.5) with a source term.

Analogously, the energy equation is obtained as

$$\partial_t \left(e^{6\varphi} \sqrt{\frac{\det \tilde{\gamma}}{\det \hat{\gamma}}} \tau \right) + \partial_j (f_\tau)^j = s_\tau - (f_\tau)^k \hat{\Gamma}^j_{jk}$$

for

$$\tau := W^2\rho_0 h - P - d \qquad \text{internal energy seen by normal observer}$$

and, with more effort, the Euler equation

$$\partial_t \left(e^{6\varphi} \sqrt{\frac{\det \tilde{\gamma}}{\det \hat{\gamma}}} S_i \right) + \partial_j (f_S)_i{}^j = (s_S)_i + (f_S)_k{}^j \hat{\Gamma}^k_{ji} - (f_S)_i{}^k \hat{\Gamma}^j_{kj}$$

for

$$S_i := \alpha T_i{}^t = W^2 \rho_0 h v_i \qquad \text{momentum density seen by normal observer}$$

For the definitions of the fluxes and the source terms in these cases the reader is referred to [MBM14].

Apart from removing tensor densities of non-zero weight, this formulation has a numerical advantage. A well-known problem concerning the Euler equation in non-Cartesian coordinates is that even in the absence of any flow the fluxes are non-zero due to a(n albeit spatially constant) pressure term. Analytically, this term is canceled by the source term such that the quantities do not change. On Cartesian grids, the Riemann solver performs the calculation exactly, as the two states of the Riemann problem are precisely the same. However, on curvilinear grids the flux is modified by a geometric factor, and the Riemann problem becomes non-trivial. Evidently the cancellation does not happen accurately any more; on a spherical polar grid typically errors grow fastest in the vicinity of the origin and make the code crash. Although but a specific setup the ability of the code to deal with it correctly is considered of paramount importance for the overall performance. In the approach presented here these terms are canceled by the background metric determinant because of (22) and the fluxes become spatially constant again.

2.8 Summary

The 3+1 decomposition is assumed to be possible for a large variety of physically relevant spacetimes. After the decomposition of the Einstein equations one ends up with conditions for every hypersurface (i.e. for the initial data) and with prescriptions about how the quantities vary from hypersurface to hypersurface. This is a very familiar situation, comparable for example with incompressible hydrodynamics in 3 dimensions, which involves one constraint and one evolution equation. The mathematical structure of the equations is, however, very different and depends on the way additional variables are introduced and information from the constraint equations is built into the evolution equations. The same is true with respect to the performance in numerical simulations. In this case coordinates are typically evolved in time: whereas α expresses how the proper time of an Eulerian observer varies from slice to slice, β reflects the coordinate evolution from slice to slice. Physics cannot provide evolution prescriptions for α and β.

3 Numerics of hyperbolic conservation laws

> Attempts to solve partial differential equations by
> finite-difference methods often end in disaster.
> C.W. Hirt, [Hir68]

3.1 Weak solutions

True discontinuities are not expected to exist in physics[2]. In hydrodynamics the observed phenomenon of a shock wave is in this sense not an exception (the transition zone being roughly of the size of the mean free path). Despite them not being discontinuous (and belonging to scales not resolvable by a continuum approach), the usual mathematical model of hydrodynamics can be adjusted to encompass discontinuous solutions that turn out to predict the behaviour of shock waves very well.

It was observed that (systems of) nonlinear conservation laws

$$\partial_t q(t,x) + \operatorname{div} f(q(t,x)) = 0, \qquad q : \mathbb{R}^+ \times \mathbb{R}^n \to \mathbb{R}, \quad f : \mathbb{R}^n \to \mathbb{R}^n \tag{27}$$

may, for given smooth initial data $q(0,x)$, not admit smooth solutions for all times and develop discontinuities.

The need for discontinuous (and thus non-differentiable) solutions to partial differential equations made an extension of the notion of a *solution* necessary. As in distribution theory the central idea is to integrate over test functions. Multiply equation (27) (setting $n = 1$ to save a tree) by $\varphi \in C^1$, a differentiable function that shall vanish outside $x \in]a,b[$ and for $t \geq T$, and integrate over it:

$$\begin{aligned} 0 &= \int_a^b \int_0^T \Big[\partial_t q(t,x) + \partial_x f(q(t,x))\Big]\varphi(t,x)\,\mathrm{d}x\mathrm{d}t \\ &= -\int_a^b q(0,x)\varphi(0,x) - \int_a^b \int_0^T u(t,x)\partial_t\varphi(t,x) + f(q(t,x))\partial_x\varphi(t,x)\,\mathrm{d}x\mathrm{d}t \end{aligned} \tag{28}$$

Being valid for classical solutions, this result can be used to define a *weak solution*, i.e. any bounded and measurable (for the integrals to exist) function $q(t,x)$, such that (28) is true for all φ as defined above. Further discussion of this concept can be found in [Smo83]. Note that weak solutions are in general not unique.

System (27) is called (strongly) hyperbolic, if any real linear combination of the Jacobian matrices $\partial f_i/\partial q$ is diagonalizable and the eigenvalues are (distinct and) real. Physically, these eigenvalues express the existence of finite information propagation speeds.

[2] In the sense that given some discontinuity that arises in a mathematical model of some real world problem it is expected that there exists a more complete model which does not contain the discontinuity any more.

It is to be noted that the hyperbolic part of the Einstein equations (see Section 2.4.5) is an example of a system of nonlinear equations that does *not* develop discontinuous solutions from smooth initial data, because, in contrast to the Euler equations, the "derivative" of the discontinuous quantity is not multiplied by this quantity again ([BPL05], Sec. 1.2.3). This is reflected in the notions of being *genuinely nonlinear* or merely *linearly degenerate*. In the latter case discontinuities do not arise from smooth initial data, and if present from the beginning, propagate as contact discontinuities and not as true shocks.

3.2 Discretization and notion of convergence

The concept of a limit, central to the domain of analysis, cannot be easily taken over by the computer. Although there exist programs able to handle formulae symbolically and to compute limits, derivatives and integrals, they are not yet able to derive general solutions to the hydrodynamical or Einstein equations. The usage of a computer restricts itself to approximations, a domain called numerical analysis. If the code shall be general, one faces two different problems – how to express a function, if not by symbols and how to compute an approximation to the solution of a differential equation, i.e. by what to replace derivatives.
The first problem can be solved by at least two different approaches: a function is given either by a finite number of point values or by a finite number of expansion coefficients in a given basis, both processes called *discretization*. The usage of the second method is the prerogative of spectral methods. We stick here in principle to the first one, and compute values on fixed positions in space, a computational *grid*, and at (not necessarily equidistant) points in time. The distance between adjacent points in time is called a *time step* and is normally denoted by Δt. The distance between adjacent points on the same coordinate is called analogously, depending on how the coordinate is called. In this introductory chapter Δx will serve as a generic grid spacing. The conceptual difference between the exact solution $q(t, x)$, the numerical continuous solution $\hat{q}(t, x)$ (unknown) and point values (e.g.) $q_i^n = \hat{q}(n\Delta t, i\Delta x)$ can be made explicit in notation, but is often suppressed (see Fig. 2). Of course the number of spatial indices has to match that of the spatial dimensions and the position of the i-th cell may be slightly different according to the application. $\Delta x(i + 1/2)$ is much in use. Note that indices[3] referring to time are the upper ones.

The way a function is approximated clearly influences the possible choices of an approximation to a derivative. First of all however, given only a finite number of point values of a general function, there is no way to calculate its derivative, as the concept of a derivative needs not only the point, but an open neighbourhood. In fact, it is impossible even to find out, whether the function is differentiable. Given a finite number of points it is always possible to construct both a smooth function and a function with as many discontinuities as one wishes. As is also well known just the smooth function passing through a finite number of points is not unique (e.g. if there is a polynomial going

[3]Confusion with differential geometric indices is not possible, because explicit discretization formulae for geometric quantities will never be written down.

through all the points, there is a countable infinity of others of higher degree doing the same).

If more information is given about the functions that are to be approximated, it might be known that derivatives exist and it is possible to find approximations to them. A standard assumption, silently assumed in many treatments of finite differencing, is that the true function is real analytic, i.e. a function f whose Taylor series

$$T[f] := \sum_{k=0}^{\infty} \frac{1}{k!} (\partial_x^k f)(x_0)(x - x_0)^k$$

in x_0 exists for all x_0 in its domain of definition and converges to $f(x)$ in a neighbourhood of x_0. Clearly, f must be smooth.
One pathological example is the analytic function $(1+x^2)^{-1}$*, which is smooth, but a Taylor series in* 0 *does not converge outside* $|x| > 1$*. This explains why the definition assumes convergence only in a neighbourhood of* x_0*. Another one,* $e^{-1/x}$ *(for* $x > 0$*), can be continously, in fact smoothly, extended to be zero for all* $x \leq 0$*, and thus can be made smooth on the whole real line, but turns out not to be analytic in 0. There, its Taylor series must vanish identically, thus existing and converging, but failing to converge against* $f(x)$ *in any neighbourhood of 0. There also exist functions, that are smooth and non-analytic everywhere. Note that even a countably infinite number of points is not sufficient to identify a unique analytic function passing through all of them. For example there is an infinity of* cos*-functions passing through the points* $\{(2\pi n, 1) : n \in \mathbb{Z}\}$.

The class of analytic functions is rather restricted, and for the same reason a standard tool in numerical analysis. Assuming $T[f](x) = f(x)$ one can for example calculate error bounds for the forward finite differencing:

$$\frac{f(x+h) - f(x)}{h} = \sum_{k=1}^{\infty} \frac{1}{k!} (\partial_x^k f)(x)(h)^{k-1} = (\partial_x f)(x) + \mathcal{O}(h)$$

where $f \in \mathcal{O}(F)$ means $\limsup_{x\to\infty} \frac{f}{F} < \infty$, i.e. the asymptotic behaviour of f and F is the same but for a finite factor. Having an approximation $\mathcal{O}(h^r)$ will be paraphrased as having an *r-th order method* or converging at *r-th order*. For analytic functions an approximation in the sense of a Taylor series is the same as the derivative of the interpolating polynomial (of suitable degree). For non-analytic functions an interpolation is in principle still possible, but no error bounds or convergence rates can be given[4].

As a matter of vocabulary, the points used for approximating a certain quantity (e.g. x and $x + h$ for the derivative at x above) are referred to as a *stencil*.

[4]Here convergence refers to the limit $\Delta x \to 0$. Another important limit is the study of how a function is approximated by polynomials of increasingly higher order, without changing Δx. For continuous functions, the Stone-Weierstrass theorem guarantees the existence of a sequence of polynomials that converge uniformly. Unfortunately, it is easy to find examples where sequences of polynomials interpolating a smooth function on *equally spaced* sampling points do not converge at all (Runge's phenomenon).

3.3 Total variation

The above way to think about convergence was heavily making use of analytic functions. The discontinuous solutions arising in nonlinear conservation laws are, contrary to how they have been defined, not treated differently from the differentiable ones when it comes to numerics. Applying the same formulae then leads to errors similar to the oscillatory Gibbs phenomenon known from Fourier series approximations of a discontinuity. To measure these oscillations the concept of *Total Variation* (TV) has been introduced. Given a set of point values $q_i \in \mathbb{R}$ it is defined as

$$\mathrm{TV}(q) = \sum_{i \in I} |q_{i+1} - q_i|$$

where the sum extends over an appropriate index domain I. For simple, i.e. linear conservation laws this notion gives useful tools for constructing methods that avoid spurious oscillations at discontinuities, as it turns out that the true solution is such that its[5] TV decreases with time. This property is called TVD (Total Variation Diminishing, actually meaning non-increasing) and has been used widely since [Har83]. An extension of this method to systems of nonlinear conservation laws is difficult, because the true solution is itself not TVD, as can be seen in certain shock collision solutions. An incorrectly oscillatory behaviour can not only affect relevant parts of the flow and thus possibly alter the results of a simulation, it can also make the density or the pressure violate their positiveness conditions, thus making the code crash.

This problem is responsible for the fact that even the simplest first-order schemes are not proven to converge for general systems of conservation laws. A discussion of these problems can be found in [LeV02]. Thus, although one cannot expect a method to perform well in hydrodynamics, if it does not for linear conservation laws, once it is doing well on them, one has to hope that it also will in the nonlinear case. An extensive testing of the code increases the confidence, but cannot give absolute guarantee.

3.4 Stability

Stability of hyperbolic conservation laws is a concept tightly related to what in real life is called causality. The word itself comes from the fact, that for certain values of $C := \Delta x/\Delta t$ the numerical solution is found to increase in absolute value without bound. For a linear equation a plane wave analysis can be performed, thus identifying the unstable modes and conditions on C. Physically speaking C is a velocity and typical results of this plane wave analysis can be interpreted as conditions that the fastest waves shall not be faster than C, i.e. shall not cross more than one cell in one time step. This view is of limited use when applied in the context of implicit time integration (see Section 3.7). Also in non-Cartesian geometries of the grid this view should not be taken too seriously. The condition relating Δx with Δt is called *Courant(-Friedrichs-Lewy)-* or *CFL-condition* [CFL28].

[5]The total variation of arbitrary functions invokes the same formula over all subdivisions of the real line (in order to account for possible discontinuities present), and takes the sup of them. For differentiable functions it reduces to the $\mathcal{L}^1$-norm of the derivative.

Additionally the stencil must be oriented in such a way, that information is taken from upstream regions. This is referred to as *upwinding*, and implies some effort when dealing with nonlinear systems, as they might not have one single direction of information propagation. [vL06] is an interesting review of arguments in favor of upwinding.

Stability, just as convergence, is much easier to show for scalar problems. An extensive discussion of various stability concepts can be found in [LeV02]; for general systems, however, again no method is proven to be stable.

3.5 Conservativity, entropy and Riemann solvers

One algorithm that has attracted a lot of interest has been proposed by Godunov in 1959 ([God59]). It is the prototypical finite volume method. The idea is to integrate the conservation law over a cell[6] $\mathcal{C} =: [x_{i-\frac{1}{2}}, x_{i+\frac{1}{2}}]$ and a time step $[t^n, t^{n+1}]$ to obtain the integral form of Eq. (27):

$$\int_{\mathcal{C}} q(t^{n+1}, x)\,\mathrm{d}x - \int_{\mathcal{C}} q(t^n, x)\,\mathrm{d}x + \int_{t^n}^{t^{n+1}} f(q(t, x_{i+\frac{1}{2}})\,\mathrm{d}t - \int_{t^n}^{t^{n+1}} f(q(t, x_{i-\frac{1}{2}})\,\mathrm{d}t = 0$$

or, defining cell and flux averages,

$$\langle q^n \rangle := \frac{1}{\Delta x} \int_{\mathcal{C}} q(t^n, x)\,\mathrm{d}x$$
$$\bar{f}_{i+\frac{1}{2}} := \frac{1}{\Delta t} \int_{t^n}^{t^{n+1}} f(q(t, x_{i+\frac{1}{2}})\,\mathrm{d}t$$

one has

$$\frac{\langle q^{n+1} \rangle - \langle q^n \rangle}{\Delta t} + \frac{\bar{f}_{i+\frac{1}{2}} - \bar{f}_{i-\frac{1}{2}}}{\Delta x} = 0$$

which, although being an exact expression, looks very much like a discretized equation. The paradigm is, via this procedure, to give the discrete numerical values a precise meaning, namely that of cell-averaged quantities. The change of the cell average (or content) is given by time-integrated fluxes over the boundaries. All of the numerics then lies in their approximation. A scheme following this procedure is called *conservative* or *in conservation form*.

A theorem by Lax and Wendroff ([LW60]) states that the numerical solution, if it converges, converges to a weak solution of the conservation law in the limit of vanishing grid spacing, provided it is computed with a conservative method (further details can be found in the proof given in [LeV02], Chapter 12). If the weak solution is not unique, then different grid refinement sequences may converge to different solutions. The wish for a physically relevant solution to be unique can be expressed via an *entropy condition*, inspired by the Second Law of Thermodynamics, because it turns out that in gas dynamics uniqueness can be achieved by discarding all shocks which are decreasing the entropy.

[6] x_i is taken to refer to the cell center and the one-dimensional grid is assumed equidistant.

Entropy conditions may also be obtainable for equations without a thermodynamic context. In general, if the weak solution becomes unique and it is possible to show that by refining the grid the numerical solution always will fulfill the entropy condition (*entropy consistency*), the Lax-Wendroff theorem implies convergence to the physically relevant solution. Still however, the numerical solutions need to first converge at all.

Godunov proposed to calculate the fluxes from the solution of the Riemann problem at each cell boundary, the two constant states involved being taken to be the cell averages. The solution to Riemann problems in hydrodynamics turns out to depend only on x/t, x being the distance from the initial discontinuity, where the flux must be constant for all times. This simplifies the calculation a lot, as the time-averaging can be performed formally without knowing the exact solution. The same procedure can be worked out for linear scalar conservation laws and reduces to first-order schemes known as *donor-cell methods*. It also incorporates upwinding and stability conditions automatically and has been shown to be entropy consistent. An algorithm calculating the flux at the cell boundaries by solving local Riemann problems is called a *Riemann solver*.

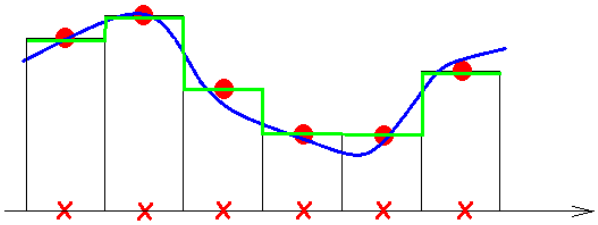

Figure 2: Summary of the discretization procedure. Blue line: Exact solution $q(t, x)$. Red dots: numerical solution q_i^n defined on a discrete subset of the real line (marked by crosses). In a conservative setting these values are given the meaning of cell averages. The introduction of a numerical continuous solution ($\hat{q}(t, x)$, green line), somehow inferred from the discrete one, is often a good way to come up with a numerical scheme. In Godunov's method it is taken to be piecewise constant. Exact solutions of the resulting Riemann problems at cell boundaries as well as subsequent averaging are used. Higher order methods would employ polynomial interpolation of the cell averages and would have to treat more complicated, generalized, Riemann problems.

Subsequently approximate Riemann solvers came up, e.g. Roe's [Roe81] and the HLL-family [HLL83]. It is clear that using cell averages as input for the Riemann problem is a crude approximation (responsible for the scheme to be only first-order accurate). The effort of calculating an exact solution out of approximate data has been recognized as unnecessary and approximate Riemann solvers are often used instead of the exact ones.

3.6 Higher-order methods

In order to increase the order of the scheme a procedure called *reconstruction* is invoked, first proposed in a series of papers presenting second order schemes by van Leer [vL73]–[vL79], and independently by [Kol11], with subsequent increases of the order: PPM [CW84] (third order), ENO/WENO [HEOC87], [SO88], DG [CS98], ADER [DET07] (arbitrary order). The only information known when using a conservative scheme are the

cell averages – how the function varies inside the cell thus cannot be uniquely determined and the generalized Riemann problem (non-constant states separated by a discontinuity) cannot be posed.

Although a true reconstruction is not possible, a(n educated) guess of the subgrid structure may lead to higher order performance. Here again highly satisfactory results can be obtained for linear conservation laws. Naturally one assumes a subgrid model of increasingly high-order polynomials, such that they interpolate the known averages over a certain number of cells. This is sometimes referred to as *conservative interpolation*. Thus, the subgrid model in one cell depends on the cell averages in the neighbouring cells. The solution of such polynomial Riemann problems can be worked out for linear equations; for hydrodynamics very often the adapted procedures, e.g. in [vL79], [CW84], are to take the values at the boundary, change them by some kind of predictor step and use them as input in the Riemann solver as if they were the two constant states of a usual Riemann problem. There exist generalized Riemann solvers, computing the solution for higher order polynomials ([BAF84] , [TMN01]), but they are computationally more involved. Certain methods ([HEOC87], [SO88], [LOC94]) do not use Riemann solvers and can more easily be extended to higher order.

In order to avoid the oscillatory behaviour, naturally appearing when a polynomial is interpolated over a discontinuity, heuristic algorithms recognize potentially unwanted oscillations (in the framework of TVD) and reduce the order of the subgrid interpolation back to constant states. It is of course not possible, given only finitely many values, to distinguish a steep slope from a discontinuity; thus there seems no hope for a non-heuristic approach to be found. TVD schemes typically perform worse at local extrema.

3.7 Time integration

Time is different from the spatial coordinates because of the nature of the equations: the Cauchy problem that one is normally facing in hydrodynamics means for many practical applications knowing the solution everywhere[7] in the spatial domain at one point in time. Thus, one must differentiate in space and integrate in time, i.e. just one-dimensionally, and Runge-Kutta (RK) schemes suggest themselves. This method is sometimes referred to as *method of lines*. Even for a given order, there are different families of Runge-Kutta schemes, and some of them have been suggested to perform better with hyperbolic PDE, as e.g. the TVD-RK schemes in [GS98]. Apart from the order an important distinction of RK-schemes is whether they are explicit or implicit ones. The former give the solution at the next time step as a function of the solution at a number of previous ones, whereas implicit schemes relate the solution at the next time step to those of the previous ones in a non-explicit manner (hence the name). Consider for example forward differencing in time of the ODE $\frac{\mathrm{d}}{\mathrm{d}t}a(t) = f(t, a(t))$, where $a(t)$ is the unknown function and we call a^n a numerical solution at time $t^n = n\Delta t$. There are two first-order possibilities to discretize in time:

$$a^{n+1} - a^n = \Delta t f(t^n, a^n) \qquad \text{or} \qquad a^{n+1} - a^n = \Delta t f(t^{n+1}, a^{n+1})$$

[7] In general the initial data must be provided for one hypersurface.

where the latter one cannot be solved explicitly for a^{n+1} for general f. The advantage of implicit RK-schemes is that they often remain stable with unconstrained Δt, but it should still be chosen sufficiently small enough in order to resolve the time-variation of the flow. This time step however might still be much larger than cell-crossing times of sound waves. Of course, in general, they need additional time to perform the implicit integration, and the question of superiourness cannot a priori be answered in favor of one or the other scheme. As will be discussed later (see Section 4.2), certain difficulties in spherical polar coordinates can be overcome by using a scheme that is partially implicit, but does not need additional iterations to be performed.

3.8 Multiple dimensions

Following the tradition of textbooks on numerical methods in hydrodynamics most of time has been spent explaining the concepts for spatially one-dimensional equations, which are rarely of big practical interest. Given the divergence of the flux, the time integration in any number of spatial dimensions however proceeds as before when using RK-schemes. The only truly new problem is that if multidimensional discretization of derivatives. In finite difference codes it is basically just a matter of bookkeeping. Here, truly multi-dimensional stencils are possible, as they are in use for the discretization of the Laplacian. For finite volume methods, unfortunately, multi-dimensional Riemann solvers are complicated and expensive even for linear equations and one is usually forced to solve three one-dimensional Riemann problems instead.

In the early days of time integration, one could quickly augment a given one-dimensional hydrodynamics code to a multi-dimensional one by making consecutive one-dimensional time integration steps for each direction, something called *directional splitting*. This has become obsolete with RK-schemes, but a certain dimensional splitting is still present at the level of Riemann solvers.

Multi-dimensional equations typically are given as systems, and thus less theoretical knowledge is available about the schemes that are used.

3.9 Summary

Numerical methods in hydrodynamics and relativity are extensively used because of the complexity of the equations. Since the 1970s a lot of effort has been put into the development of numerical schemes that resolve shocks sharply and automatically. This has also given time to fill the theoretical gap of missing convergence proofs by extensive practical performance studies.

When it comes to compressible gas dynamics the derivatives must be approximated by special procedures. Given the interpretation as a conservation law even for the discretized equation, the numerical values are seen as cell averages. To compute a function that interpolates them is a slightly different procedure than interpolating point values. Because of the possible presence of discontinuities very steep changes in the computed values are interpreted as shocks and low-order interpolations are employed there in order to avoid oscillatory behaviour.

In pure spacetime evolution neither the interpretation as conservtion law is used in practice nor are there discontinuous solutions to be treated differently. Thus the usual finite difference formulae can be used directly, central and at least fourth-order schemes are found to give good results.

4 Spherical polar coordinates and the Yin-Yang grid

Why with the time do I not glance aside
To new-found methods and to compounds strange?
William Shakespeare, Sonnet 76

4.1 Geometry of the Yin-Yang grid

The Yin-Yang grid [KS04] is depicted in Fig. 3. For every 2-sphere in the spherical polar grid the patch consisting of

$$(\vartheta, \varphi) \in \left[\frac{\pi}{4}, \frac{3\pi}{4}\right] \times \left[\frac{\pi}{4}, \frac{7\pi}{4}\right]$$

covers its complement when subject to rotation

$$\mathfrak{R} := \begin{pmatrix} -1 & & \\ & & 1 \\ & 1 & \end{pmatrix} = \mathfrak{R}_z(\pi) \circ \mathfrak{R}_x\left(\frac{\pi}{2}\right)$$

with $\mathfrak{R} \in SO(3)$ and self-inverse.
Each patch has an area of $\frac{3}{\sqrt{2}}\pi \approx 0.53 \cdot 4\pi$.

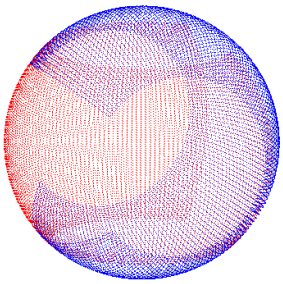

Figure 3: The two patches of a Yin-Yang grid.

The two patches define two coordinate systems for points on the sphere. Indeed, the rotation so far moving *one* point on the sphere can be equally thought of as relating two different points, which have the same values of angular coordinates in two different coordinate systems. The position of every point on the sphere can be expressed with two different angles:

$$r \begin{pmatrix} \cos\varphi \sin\vartheta \\ \sin\varphi \sin\vartheta \\ \cos\vartheta \end{pmatrix} = \begin{pmatrix} x \\ y \\ z \end{pmatrix} = r \begin{pmatrix} -\cos\tilde{\varphi} \sin\tilde{\vartheta} \\ \cos\tilde{\vartheta} \\ \sin\tilde{\varphi} \sin\tilde{\vartheta} \end{pmatrix} = r\,\mathfrak{R} \begin{pmatrix} \cos\tilde{\varphi} \sin\tilde{\vartheta} \\ \sin\tilde{\varphi} \sin\tilde{\vartheta} \\ \cos\tilde{\vartheta} \end{pmatrix}$$

Because of $\mathfrak{R}^2 = \mathfrak{id}$ it is not necessary to specify which patch shall use the tilded quantities.

From this equality different kinds of relations between the two sets of angles can be deduced:

$$\cos\tilde{\vartheta} = \sin\varphi \sin\vartheta, \text{ and also } \cos\vartheta = \sin\tilde{\varphi} \sin\tilde{\vartheta} \tag{29}$$

$$\cos\tilde{\varphi} = \frac{-\cos\varphi \sin\vartheta}{\sin\tilde{\vartheta}} \quad \text{which gives} \quad \frac{\cos\tilde{\varphi}}{\sin\vartheta} = -\frac{\cos\varphi}{\sin\tilde{\vartheta}}$$

$$\tan\tilde{\varphi} = \frac{\cos\vartheta}{-\cos\varphi \sin\vartheta} \quad \text{as well as} \quad \tan\varphi = \frac{\cos\tilde{\vartheta}}{-\cos\tilde{\varphi} \sin\tilde{\vartheta}} \tag{30}$$

all of which can be found by considering certain components of the vectors or dividing them by each other.

In order to obtain the transformation matrix for vector components write first down the unit vectors: $e_r = e_{\tilde{r}}$,

$$e_\vartheta = \begin{pmatrix} \cos\varphi\cos\vartheta \\ \sin\varphi\cos\vartheta \\ -\sin\vartheta \end{pmatrix}, \quad e_{\tilde{\vartheta}} = \begin{pmatrix} -\cos\tilde{\varphi}\cos\tilde{\vartheta} \\ -\sin\tilde{\vartheta} \\ \sin\tilde{\varphi}\cos\tilde{\vartheta} \end{pmatrix}, \quad e_\varphi = \begin{pmatrix} -\sin\varphi \\ \cos\varphi \\ 0 \end{pmatrix}, \quad e_{\tilde{\varphi}} = \begin{pmatrix} \sin\tilde{\varphi} \\ 0 \\ \cos\tilde{\varphi} \end{pmatrix}$$

and note the following identity

$$v = v^r e_r + v^\vartheta e_\vartheta + v^\varphi e_\varphi = v^{\tilde{r}} e_{\tilde{r}} + v^{\tilde{\vartheta}} e_{\tilde{\vartheta}} + v^{\tilde{\varphi}} e_{\tilde{\varphi}}$$

for arbitrary vector v.

The special case $v^\vartheta = v^\varphi = 0$ gives $v^r = v^{\tilde{r}}$, because $e_{\tilde{r}} = e_r$ and both frames are orthonormal. It is useful to consider the y-component of this vector equation first because it does not involve $e_{\tilde{\varphi}}$:

$$\begin{aligned} -v^{\tilde{\vartheta}}\sin\tilde{\vartheta} &= v^\vartheta \sin\varphi\cos\vartheta + v^\varphi\cos\varphi \\ v^{\tilde{\vartheta}} &= -v^\vartheta\frac{\sin\varphi\cos\vartheta}{\sin\tilde{\vartheta}} - v^\varphi\frac{\cos\varphi}{\sin\tilde{\vartheta}} = -v^\vartheta\sin\varphi\sin\tilde{\varphi} - v^\varphi\frac{\cos\varphi}{\sin\tilde{\vartheta}} \end{aligned}$$

where $\cos\vartheta = \sin\tilde{\varphi}\sin\tilde{\vartheta}$ was used for the last equality.

Consider now the combination $v^x\sin\tilde{\varphi} + v^z\cos\tilde{\varphi}$, which is, up to the decoupling r-subspace

$$\begin{aligned} v^{\tilde{\varphi}} &= v^\vartheta(\sin\tilde{\varphi}\cos\varphi\cos\vartheta - \cos\tilde{\varphi}\sin\vartheta) + v^\varphi(-\sin\tilde{\varphi}\sin\varphi) \\ &= v^\vartheta\left(\frac{\cos^2\vartheta}{\sin\tilde{\vartheta}}\cos\varphi + \frac{\cos\varphi\sin^2\vartheta}{\sin\tilde{\vartheta}}\right) + v^\varphi(-\sin\tilde{\varphi}\sin\varphi) \\ &= v^\vartheta\frac{\cos\varphi}{\sin\tilde{\vartheta}} + v^\varphi(-\sin\tilde{\varphi}\sin\varphi) \end{aligned}$$

where $\sin\tilde{\varphi} = \cos\vartheta/\sin\tilde{\vartheta}$ and $\cos\tilde{\varphi} = -\cos\varphi\sin\vartheta/\sin\tilde{\vartheta}$ were inserted. This finally gives the matrix

$$\begin{pmatrix} v^{\tilde{r}} \\ v^{\tilde{\vartheta}} \\ v^{\tilde{\varphi}} \end{pmatrix} = \begin{pmatrix} 1 & 0 & 0 \\ 0 & -\sin\varphi\sin\tilde{\varphi} & -\cos\varphi/\sin\tilde{\vartheta} \\ 0 & \cos\varphi/\sin\tilde{\vartheta} & -\sin\tilde{\varphi}\sin\varphi \end{pmatrix} \begin{pmatrix} v^r \\ v^\vartheta \\ v^\varphi \end{pmatrix} =: \mathfrak{M}\begin{pmatrix} v^r \\ v^\vartheta \\ v^\varphi \end{pmatrix} \tag{31}$$

Another way to think of the matrix is to use the basis vectors e_r, e_ϑ, e_φ:

$$v^{\tilde{\beta}} = e^{\tilde{\beta}}{}_\alpha v^\alpha$$

where the element $e^{\tilde{\beta}}{}_\alpha$ stands in the $\tilde{\beta}$-row and in the α-column:

$$(e^{\tilde{\beta}}{}_\alpha) = \begin{pmatrix} e^{\tilde{r}}{}_r & e^{\tilde{r}}{}_\varphi & e^{\tilde{r}}{}_\vartheta \\ e^{\tilde{\vartheta}}{}_r & e^{\tilde{\vartheta}}{}_\varphi & e^{\tilde{\vartheta}}{}_\vartheta \\ e^{\tilde{\varphi}}{}_r & e^{\tilde{\varphi}}{}_\varphi & e^{\tilde{\varphi}}{}_\vartheta \end{pmatrix}$$

and the indices run over the r, ϑ, φ-coordinates.

$e^{\tilde{\beta}}{}_{\alpha}$ also is the $\tilde{\beta}$-component of the e_α unit vector.

The property $\dfrac{\cos\tilde{\varphi}}{\sin\vartheta} = -\dfrac{\cos\varphi}{\sin\tilde{\vartheta}}$ assures that the inverse transformation is obtained by just changing from primed quantities to unprimed ones. It acts as

$$v^{\alpha} = e^{\alpha}{}_{\tilde{\beta}} v^{\tilde{\beta}}$$

with the same convention, that the first (or upper) index denotes the row. $\mathfrak{M}$ is orthogonal, i.e. its inverse is the transpose ($\mathfrak{M}^{-1} = \mathfrak{M}^{\mathrm{T}}$). Due to its special structure the inverse has the same elements but for a sign off the diagonal:

$$e^{\alpha}{}_{\tilde{\alpha}} = e^{\tilde{\alpha}}{}_{\alpha} \quad e^{\alpha}{}_{\tilde{\beta}} = -e^{\tilde{\beta}}{}_{\alpha} \quad \text{whenever } \alpha \neq \beta$$

Covariant tensors of rank 2 (like the metric) transform via

$$g_{\tilde{\mu}\tilde{\nu}} = g_{\mu\nu} e^{\mu}{}_{\tilde{\mu}} e^{\nu}{}_{\tilde{\nu}}$$

using the inverse transformation:

$$\tilde{g} = \mathfrak{M}^{-1^T} g \mathfrak{M}^{-1} = \mathfrak{M} g \mathfrak{M}^{-1}$$

As each patch, once set up, is by itself a part of (mutually misaligned) spherical polar coordinate systems, the evolution of the quantities is unaffected by the introduction of a Yin-Yang grid and is performed as it is described in [BMCCM13]. The time integration differs only by the choice of the time step (4.2). Additional effort is needed to ensure communication between the two grids (Sec. 4.3) and during initialization (Sec. 4.4). Specific implementation details are given in Sec. 4.5.

4.2 Time step and integration

Spherical polar coordinates make various divergent factors, e.g. $\frac{1}{r}$, appear in the equations. It has been found ([CCCD12]) that the stability of the time evolution of such terms can be dramatically improved by introducing a Runge-Kutta method which is not fully explicit. Consider for example the following system for two unknown functions u and v:

$$\begin{aligned} \partial_t u &= R_1(u, v) \\ \partial_t v &= S(u) + R_2(u, v) \end{aligned} \tag{32}$$

with R_1 and R_2 being numerically well-behaved in u and v (call them regular) and S shall contain the unstable terms (singular or stiff). Observe that S is assumed to depend only on u, a fact tailored to the real application at hand to be discussed shortly.

The first part of the system is to be evolved explicitly, e.g. for a first order RK:

$$u^{n+1} = u^n + \Delta t R_1(u^n, v^n)$$

For the second part there is the choice whether to use u^{n+1} or u^n. Observe that there is no difference in computational cost. It is found that the scheme is performing in a much better way, when the singular terms are evolved with the updated value u^{n+1}:

$$v^{n+1} = v^n + S(u^{n+1}) + R_2(u^n, v^n)$$

This method is called *PIRK* (*P*artially *I*mplicit *RK*).

The 2nd-order version

$$\begin{aligned}
u^{n+1/2} &= u^n + \Delta t R_1(u^n, v^n) \\
v^{n+1/2} &= v^n + \Delta t \left(\frac{1}{2} S(u^n) + \frac{1}{2} S(u^{n+1/2}) + R_2(u^n, v^n) \right) \\
u^{n+1} &= \frac{1}{2} \left(u^n + u^{n+1/2} + \Delta t R_1(u^{n+1/2}, v^{n+1/2}) \right) \\
v^{n+1} &= v^n + \frac{1}{2} \Delta t \left(S(u^n) + S(u^{n+1}) + R_2(u^n, v^n) + R_2(u^{n+1/2}, v^{n+1/2}) \right)
\end{aligned}$$

is currently used.

In the system (11), (12), (15), (18), (21), (23), (24) and (25) the conformal metric components, the conformal factor, the lapse and the shift (in (24)) are evolved explicitly (like the quantity u in (32)). Then there are three quantities like v. First, the trace and the traceless part of the extrinsic curvature are evolved partially implicitly using the so far updated quantities. Then, secondly, the $\tilde{\Gamma}^k$ use them and the new values of the curvature for partially implicit evolution. Finally the quantities B^i are evolved partially implicitly using the updated values of all the other quantities. Lie derivatives and matter are treated explicitly. See Appendix B in [BMCCM13] for a detailed list of equations.

The CFL-condition can be taken in spherical polar coordinates as

$$\frac{c\Delta t}{\min_{\text{grid}}(\Delta r, \Delta r \Delta\vartheta, \Delta r \Delta\varphi \Delta\vartheta)} < 1 \qquad \text{(spherical polar)}$$

where c is the largest speed of information propagation, being the speed of light in relativity. When setting the value of Δt, the inequality is replaced by an equality and the right hand side by some number smaller than one, which is given the name *Courant factor*. The relevant length is inspired by the line element

$$\mathrm{d}\ell^2 = \mathrm{d}r^2 + r^2 \mathrm{d}\vartheta^2 + r^2 \mathrm{d}\varphi^2 \sin^2\vartheta$$

and is dominated by the last term, a product of three small quantities. Thus keeping the aspect ratio of the cells and increasing the resolution by a factor of two makes the code run $2^6 = 64$ times slower.

When using the Yin-Yang grid these restrictions are somewhat loosened. Observe that the crucial product of three quantities is actually $\Delta r \Delta\varphi \sin(\min_{\text{grid}} \vartheta)$, which reduces to the given form for usual spherical polar coordinates. However in a Yin-Yang grid $\sin(\min_{\text{grid}} \vartheta)$ does not depend on the resolution, being of the order of 0.7. Thus the CFL-condition is now

$$\frac{c\Delta t}{\min_{\text{grid}}(\Delta r, \Delta r \Delta\vartheta, \Delta r \Delta\varphi \sin(\vartheta))} < 1 \qquad \text{(Yin-Yang)}$$

which reduces the runtime by one order; keeping the example above, an increase by a factor of two in resolution makes the code $2^5 = 32$ times slower.

On the other hand, the theoretical speedup with respect to a code using normal spherical polar coordinates with comparable resolution is of the order of $0.44N_\vartheta$, with N_ϑ being the number of cells in ϑ-direction for a Yin-Yang code. Practically one cannot expect this value to be reached exactly (due to extra work for interpolations and the overlap region, where calculations are performed redundantly), but as this value increases with increasing resolution, the Yin-Yang grid easily gives an order of magnitude speedup.

4.3 Boundary and parity conditions

4.3.1 Outer boundary conditions

In order the problem (27) to be well-posed boundary conditions have to be supplied, either because they are needed on physical grounds or become necessary just because the domain of definition of any numerical solution cannot be but a subset of the $\mathbb{R}^3$. The domain of calculation being a sphere in the case considered, values of the quantities outside some given radius have to be provided.

For the Einstein equations Sommerfeld boundary conditions are imposed on an asymptotically flat space. This is, strictly speaking, not exactly achievable, as this concerns values at infinity. Taking the outer boundary sufficiently far away one can however hope to be able to approximate these conditions to sufficient precision.

For the hydrodynamical part sufficiently small values of the hydrodynamical quantities are assumed outside the grid, such that anything that leaves the grid would propagate outwards as a Sedov wave. This choice has not shown any undesired influence in applications. Astrophysical objects have a finite extent and outside of them some low density atmosphere[8] is assumed. This is the primary reason for defining the boundary conditions in the same way. As the outer boundary is optimally placed very far from the object, no relevant flow through it is expected.

4.3.2 Angular conditions

Due to the choice of coordinates it turns out that in comparison to a Cartesian grid more work is necessary, when using spherical polar coordinates. Further distinction must be made between polar coordinates with or without a Yin-Yang grid.

For the evaluation of stencils every cell has to have neighbouring values. Those cells that would naturally not have any neighbours are provided with so called *ghost cells* as neighbours (all others will sometimes be called valid cells). Thus during the actual calculation one does not have to modify the finite difference formulae for cells near the boundary, but provides the necessary values as fictitious neighbours.

Spherical polar grids Consider first the φ-direction and mind that in the computational space the grid has been torn apart and values at small angles do not close with

[8]Numerical hydrodynamics codes in general do not handle vacuum well.

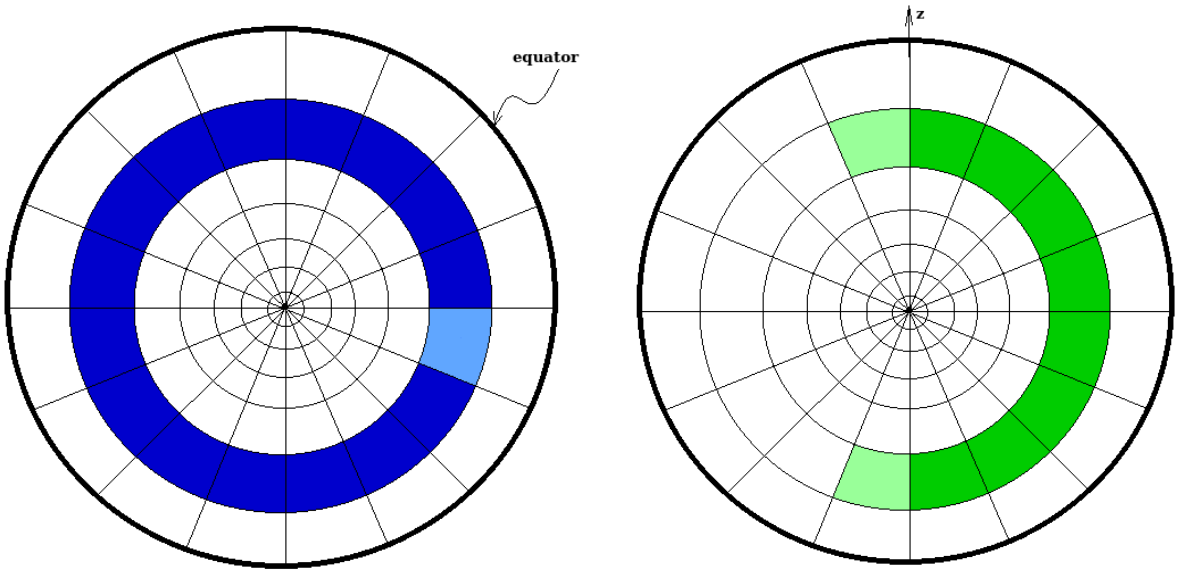

Figure 4: Illustration of angular parity conditions. (a): φ-direction. (b) ϑ-direction.

values at 2π. The cells at the lower boundary of the computational space have thus to be provided with information from the upper boundary, identifying a cell at negative angle $-\varphi$ with the cell at $2\pi - \varphi$. An analogous situation holds for cells at the upper boundary for $\varphi \geq 2\pi$.

The angular boundaries in ϑ-direction are slightly more difficult and their treatment is referred to as *axis parity conditions*. The cell located at a negative angle $-\vartheta$ and some angle φ has to be identified with the cell at $(\vartheta, \varphi + \pi)$. However, in contrast to the case of the φ-coordinate the basis of the tangent spaces to the sphere is changing discontinuously when ϑ becomes negative. Indeed, the ϑ angle is always pointing towards the North pole, and the ϑ-component of any smooth vector field experiences a switch of sign on a curve going through the pole.

The value obtained directly from $(\vartheta, \varphi + \pi)$ would still be equipped with this minus sign. However, componentwise interpolation only works when all the vectors inside the stencil are expressed in a continuously varying basis (this statement is discussed in more detail below). An extra minus sign must be given to the ϑ-component of the vector field, when filling ghost cells at the axial boundary.

Yin-Yang grid When using the Yin-Yang grid evidently both these conditions are not necessary and are replaced by conceptually simpler boundary conditions. The ghost cells of each patch are filled by looking up the corresponding values on the other patch. In general the cells of the two grids will not match exactly and the $(\tilde{\vartheta}, \tilde{\varphi})$ pair of transformed angles of some ghost cell located at (ϑ, φ) on one grid will not hit a pair of coordinates of a cell of the other grid. A certain number of cells lying around this point, however, can be used to gather information in order to interpolate a value to the desired location.

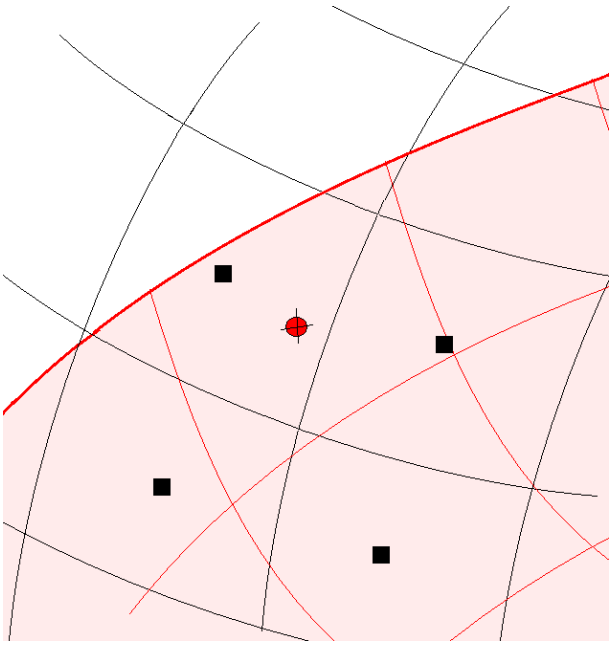

Figure 5: Illustration of the look-up procedure. The red dot denotes a cell centered at (ϑ, φ), and the black squares are the four neighbours of $(\tilde{\vartheta}, \tilde{\varphi})$.

The interpolation coefficients depend on the relative position of $(\tilde{\vartheta}, \tilde{\varphi})$ to the neighbouring cells, something known already in advance. These coefficients need to be calculated once. The usage of 4 nearest cells makes a bilinear interpolation possible, and with e.g. 16 cells a fourth order interpolation can be obtained. Note that in presence of shock waves a fourth order interpolation will produce spurious oscillations – it should not be used with hydrodynamics. For reference the formulae are given:

$$\begin{aligned}\mathcal{I}_1(y_1,\ldots,y_4;u,t) = i_2^{(1)}(u)\left[i_1^{(1)}(t)y_4 + i_2^{(1)}(t)y_3\right] \\ + i_1^{(1)}(u)\left[i_1^{(1)}(t)y_1 + i_2^{(1)}(t)y_2\right]\end{aligned}$$

with $i_1^{(1)}(x) = 1 - x$ and $i_2^{(1)}(x) = x$

$$\begin{aligned}\mathcal{I}_3(y_1,\ldots,y_16;u,t) = i_4^{(3)}(u)\left[i_1^{(3)}(t)y_{13} + i_2^{(3)}(t)y_{12} + i_3^{(3)}(t)y_{11} + i_4^{(3)}(t)y_{10}\right] \\ + i_3^{(3)}(u)\left[i_1^{(3)}(t)y_{14} + i_2^{(3)}(t)y_4 + i_3^{(3)}(t)y_3 + i_4^{(3)}(t)y_9\right] \\ + i_2^{(3)}(u)\left[i_1^{(3)}(t)y_{15} + i_2^{(3)}(t)y_1 + i_3^{(3)}(t)y_2 + i_4^{(3)}(t)y_8\right] \\ + i_1^{(3)}(u)\left[i_1^{(3)}(t)y_{16} + i_2^{(3)}(t)y_5 + i_3^{(3)}(t)y_6 + i_4^{(3)}(t)y_7\right]\end{aligned}$$

with

$$i_1^{(3)}(x) = -\frac{1}{6}x(x-1)(x-2)$$
$$i_2^{(3)}(x) = \frac{1}{2}(x+1)(x-1)(x-2)$$
$$i_3^{(3)}(x) = -\frac{1}{2}(x+1)x(x-2)$$
$$i_4^{(3)}(x) = \frac{1}{6}x(x+1)(x-1)$$

and $t := T/\Delta\vartheta$, $u := U/\Delta\varphi$ (compare Fig. 6)

Non-scalar quantities can be interpolated either componentwise or by transforming them into a spatially fixed (coordinate independent) basis, interpolating componentwise and transforming back. One defines an r-th order interpolation $\tilde{A}(x)$ from a set of values $\{(x_i, A_i)\}$ as an approximation of the true function $A(x)$ of the form

$$\tilde{A}(x) = \mathcal{I}(\{A_i\}) = A(x) + \mathcal{O}(A^{(r+1)}(x)(\Delta x)^{r+1})$$

with $\Delta x = x_{i+1} - x_i$, assumed constant for simplicity and $A(x)$ possessing sufficiently many continuous derivatives.

Then, given a vector field $v : \mathbb{R} \to \mathbb{R}^2$ on a curve parametrized by α one can express it either in a constant or in a space-dependent basis:

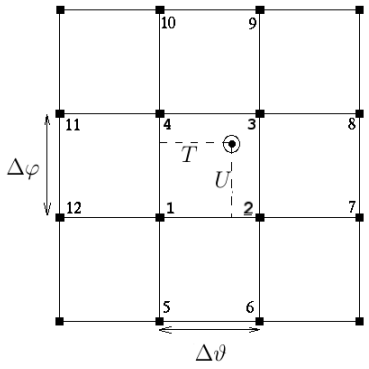

Figure 6: Points involved in the interpolation stencils.

$$v = v^x(\alpha)e_x + v^y(\alpha)e_y = v^1(\alpha)e_1(\alpha) + v^2(\alpha)e_2(\alpha)$$

where the two choices have been denoted by x, y and $1, 2$, respectively.

If the interpolation of a vectorial quantity is defined via a componentwise interpolation in a fixed basis, one obtains

$$\mathcal{I}^{\text{fixed}}(v(\alpha)) := \mathcal{I}(\{v^x(\alpha_i)\})e_x + \mathcal{I}(\{v^y(\alpha_i)\})e_y = v(\alpha) + \mathcal{O}((v^x)^{(r+1)}(\alpha)(\Delta\alpha)^{r+1}, (v^y)^{(r+1)}(\alpha)(\Delta\alpha)^{r+1})$$

Now a similar kind of relation holds for a varying basis, but the error term is:

$$\mathcal{O}((v^1)^{(r+1)}(\alpha)(\Delta\alpha)^{r+1}, (v^2)^{(r+1)}(\alpha)(\Delta\alpha)^{r+1})$$

which now involves both the continuity of the vector field and of the basis vectors, most easily observed for orthonormal bases, where $v^1 = v^x e_1^x + v^y e_2^y$. Thus, the convergence and its rate are unaltered, whether one interpolates non-scalar quantities in a fixed or varying basis, if the variation of the basis is sufficiently differentiable. However, one expects less errors being produced with the fixed-basis method.

Visually the method using the varying basis also interpolates the orientation of the basis at the intermediate point, whereas the other uses the exact basis and interpolates only the vector field. Both methods are implemented and available in the code.

Note that the interpolation is not done in a conservative manner – for this step all the values involved are considered to be point values. In view of the Lax-Wendroff-theorem this is of course highly undesirable. In [PXT06] a solution for the evolution of scalar quantities is presented which amounts to keeping track of the exact relative positions of the overlapping cells and accounting for this in the flux balance. However, fluxes of vectorial quantities remain problematic.

4.3.3 Parity conditions at the origin

The Yin-Yang grid is defined on spheres of constant r-coordinate, thus any parity or boundary conditions at the origin are unaltered by this approach and still have to be taken into account. Having two coordinate patches actually even enriches the number of conditions.

In normal spherical polar coordinates a cell at a negative radius $-r$ and at some angular position (ϑ, φ) will be identified with the positive radius r and the angular position $(\pi - \vartheta, \varphi + \pi)$. Now both the r- and φ-unit vectors discontinuously change sign and so the r- and φ-components have to be equipped with an extra minus sign (compare Fig. 7).

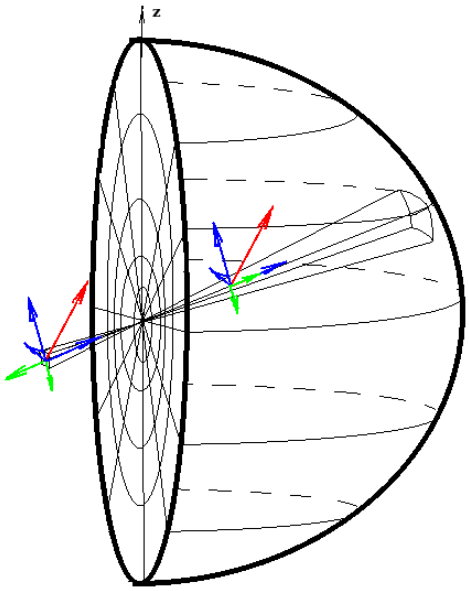

Figure 7: Radial parity conditions. In red two representatives of a constant vector field are depicted, in blue – its components along the unit vectors in spherical polar coordinates; in green e_r and e_ϑ. One observes that the projection on e_ϑ does not change sign, but the projection on e_r does. The projection onto e_φ does also change sign, but is left out in order not to overcomplicate the image.

In the Yin-Yang framework this is only true if both positions, i.e. (ϑ, φ) and $(\pi - \vartheta, \varphi + \pi)$ live on the same patch, which happens for φ sufficiently far from π. In general however one cannot expect to stay on the same coordinate patch when performing this

rotation. This means that again interpolation and transformation is needed. Once done, the same parity conditions apply. A concise version of the complete algorithm can be found in Table 2. The additional signs are given in Table 1.

		r	ϑ	φ
$-$	r	$+$	$-$	$+$
$+$	ϑ		$+$	$-$
$-$	φ			$+$

Table 1: Signs in the parity conditions at the origin for vectors and tensors.

Note that the parity conditions, at the origin or elsewhere, do not impose any symmetry. As an example one should consider the difference between insisting on (r, ϑ, φ) to be identified with $(r, \pi - \vartheta, \varphi + \pi)$ or with $(-r, \pi - \vartheta, \varphi + \pi)$. The latter case is just a continuation of formally non-allowed values of the coordinates.

One subtlety concerns the transformation of non-scalar quantities when a ghost cell with negative radius has to filled. As the transformation is space-dependent, the question may arise which position to take: the original (ϑ, φ) associated with the negative radius or $(\pi - \vartheta, \varphi + \pi)$. The latter is readily found to be the correct one.

```
1  if r < 0
2        φ ↦ φ + π, ϑ ↦ π − ϑ
3  if (ϑ, φ) inside angular domain of its patch
4        if r < 0
5              Copy values from (|r|, ϑ, φ), apply parity conditions on non-scalar quantities
6        else //Cannot occur
7  else
8        Get interpolated value from other patch using |r|, transform non-scalar quantities
9        if r < 0
10             Set values after having applied parity conditions
11       else
12             Set values as they are
```

Table 2: Algorithm for filling a ghostcell located at (r, ϑ, φ).

4.4 Initialization and output

The initial data will in the majority of the cases be given in usual spherical polar coordinates. If explicit functions of the angular coordinates are involved, then extra work has to be done to set them up on a Yin-Yang grid. In one of the patches the coordinates would coincide, while in the other one the coordinates have first to be transformed back to the usual spherical polar coordinates via Equations (30) and (29), and these latter used for the computation.

Independently of whether angles are explicitly involved, non-scalar quantities have to be transformed using (31), if they belong to a patch using different coordinates than the normal ones.

Of course, in principle the initial data may also be given in some independent coordinate system, e.g. a Cartesian one. In this case they may be transformed directly onto the right Yin-Yang patch.

It might happen that one wishes to set up derived quantities, e.g. the determinant of a metric, or some transformed quantity, although the above mentioned transformation has not been performed yet. This is only possible if the operation in question commutes with the transformation from one patch to the other. As the latter is an orthogonal one, determinant evaluation as well as basis changes can be performed before the quantity is transformed onto the respective patch. As an example consider the transformation of the metric from coordinate to orthonormal basis, which involves various factors of $\sin\vartheta$. They have in this case (i.e. before the metric is transformed) to be calculated with the angles of a usual spherical polar system, and not the angles of the future patch.

4.5 Implementation details

The data, e.g. the conserved quantities are stored in rectangular-shape arrays and accessed via coordinate indices $(i_r, i_\varphi, i_\vartheta)$. The grids are implemented as one further dimension to the existing arrays, for which the index can take one of two possible values. Although not the case in the treatment of the boundaries, there is qualitative difference between the patch whose coordinates coincide with normal spherical ones and the turned patch, for example when it comes to initial data. It is thus important to keep track of the orientation of the patches.

Call

$$\varphi_{\text{start}} := \frac{\pi}{4} \qquad \vartheta_{\text{start}} := \frac{\pi}{4}$$
$$\varphi_{\text{end}} := \frac{7\pi}{4} \qquad \vartheta_{\text{end}} := \frac{3\pi}{4}$$

Furthermore, it may be necessary to have additional overlap between the patches. Call N_{overlap} the number of cells that are added as valid cells between the patch defined above and the ghost cells, whose number N_{ghost} is determined by the needs of the finite differencing procedure. The value adapted here is $N_{\text{overlap}} = 2$.

The choice of an interval of length 2π on the real line where the angles shall lie does not affect the Yin-Yang grid by itself, $]-\pi, \pi]$ however is in agreement with the image of the `atan2`-function, built in in F90. The code described has been using $[0, 2\pi[$ before.

If the angular arrays, not counting the ghostcells, have a starting index of 1 and run

up to N_φ or N_ϑ, then one has

$$\Delta\varphi = \frac{\varphi_{\text{end}} - \varphi_{\text{start}}}{N_\varphi - 2N_{\text{overlap}}}$$

$$\Delta\vartheta = \frac{\vartheta_{\text{end}} - \vartheta_{\text{start}}}{N_\vartheta - 2N_{\text{overlap}}}$$

$$\varphi = (i_\varphi - N_{\text{overlap}} - 0.5) \cdot \Delta\varphi + \varphi_{\text{start}} \bmod 2\pi \tag{33}$$

$$\vartheta = (i_\vartheta - N_{\text{overlap}} - 0.5) \cdot \Delta\vartheta + \vartheta_{\text{start}} \bmod 2\pi \tag{34}$$

Mind that with this definition N_ϑ and N_φ denote the number of valid cells on just one patch of the Yin-Yang grid.

Sometimes it may become necessary to compare this setup with the cells in a code with usual spherical polar coordinates; possible only for one patch of course. One finds, taking ϑ as an example and calling now temporarily the grid size N^{YY} or N, depending on whether we speak of the number of ϑ-cells in a patch of a Yin-Yang code or in a full $[0, 2\pi] \times [0, \pi]$ one:

$$\frac{\pi}{4} + \frac{\pi/2}{N^{\text{YY}} - 2N_{\text{overlap}}}(i_\vartheta^{\text{YY}} - N_{\text{overlap}} - 0.5) = \frac{\pi}{N}(i_\vartheta - 0.5)$$

If one takes e.g. $j = \frac{N}{2}$, $j^{\text{YY}} = \frac{N^{\text{YY}}}{2}$, and $N_{\text{overlap}} = 2$ then this yields

$$N^{\text{YY}} = \frac{N}{2} + 4 \tag{35}$$

Recall, that when filling a cell at position $-r$ and an angular position (ϑ, φ) the cell at r and angular position $(\pi - \vartheta, \varphi + \pi)$ is accessed (Sec. 4.3). The need to turn φ by π or to reflect ϑ on the equatorial plane thus occurs quite often. In order for this procedure to work at the discretized level, i.e. the result of the operation to end up on a cell center again, certain conditions must be fullfilled by N_ϑ and N_φ. One finds:

$$\begin{aligned}\text{turnPhiByPI}(\varphi) &= \left\lfloor 0.5 + N_{\text{overlap}} + \frac{(i_\varphi - N_{\text{overlap}} - 0.5)\Delta\varphi + \varphi_{\text{start}} + \pi - \varphi_{\text{start}}}{\Delta\varphi} \right\rfloor \\ &= \left\lfloor i_\varphi + \frac{\pi}{\Delta\varphi} \right\rfloor = \left\lfloor i_\varphi + 2\frac{N_\varphi - 2N_{\text{overlap}}}{3} \right\rfloor\end{aligned}$$

Now in order for this cell to be hit exactly the expression inside the brackets must already be an integer. For $N_{\text{overlap}} = 2$ one finds the condition $N_\varphi \equiv 1 \bmod 3$.

Analogously one finds $N_\vartheta \equiv 0 \bmod 2$.

Apart from the question of how to communicate between the two patches the following issue presents itself when using overlapping grids: For the overlap zone in general two distinct solutions are calculated and one has to decide which one to take. There does not seem to exist a general principle telling which patch to take here; one of them is systematically favoured in the code described. More precisely, all cells which, by inverting (33) and (34) and using angles from the usual spherical polar coordinates, have an index

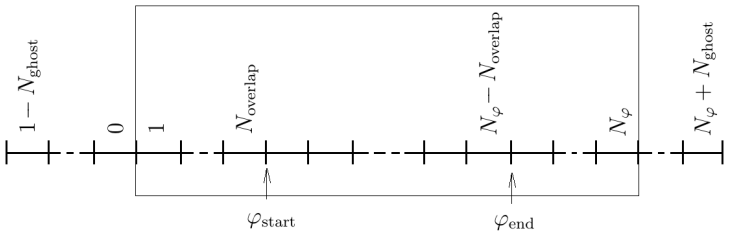

pair lying inside $[1, N_\vartheta] \times [1, N_\varphi]$ are counted as one of the patches. All other cells go into the other patch.

As can be observed from Eq. (33) and (34) the angular range corresponding to the index range $[1, N_\varphi]$ and $[1, N_\vartheta]$ is larger than $[\varphi_{\text{start}}, \varphi_{\text{end}}]$ and $[\vartheta_{\text{start}}, \vartheta_{\text{end}}]$, respectively. The number of cells in angular directions should not become too small – first of all it should never drop below $2N_{\text{overlap}}$. But furthermore, as for a small number of cells they become very big the additional overlap cells and the ghost cells (that are added around the valid cells) may make one patch close up, i.e. overlap with itself. As this would increase the bookkeeping efforts dramatically such setups are not foreseen in the code and are blocked. It is possible to make an estimate of the minimal numbers of grid cells the code needs. The angular value of the outermost ghost zone:

$$\begin{aligned}
\varphi_{\text{end}} + \Delta\varphi(N_{\text{overlap}} + N_{\text{ghost}}) &\overset{!}{<} \pi \\
\varphi_{\text{end}} + \frac{\varphi_{\text{end}} - \varphi_{\text{start}}}{N_\varphi - 2N_{\text{overlap}}}(N_{\text{overlap}} + N_{\text{ghost}}) &\overset{!}{<} \pi \\
\frac{(\varphi_{\text{end}} - \varphi_{\text{start}})(N_{\text{overlap}} + N_{\text{ghost}})}{\pi - \varphi_{\text{end}}} + 2N_{\text{overlap}} &\overset{!}{<} N_\varphi
\end{aligned}$$

or inserting the values from above

$$8N_{\text{overlap}} + 6N_{\text{ghost}} \overset{!}{<} N_\varphi$$

In practice this value may be off by some grid cells, but gives an order of magnitude. An analogous calculation for ϑ yields $4N_{\text{overlap}} + 2N_{\text{ghost}} \overset{!}{<} \text{gridSize}_\vartheta$.

If one wants to vary the grid resolution while keeping the aspect ratio of the cells as constant as possible, the following prescription for N_r, N_ϑ, N_φ can be used ($N_{\text{overlap}} = N_{\text{ghost}} = 2$):

$$N_r \text{ given}, \qquad N_\vartheta = \max\left(12, \lceil q_\vartheta N_r \rceil^{0 \bmod 2}\right), \qquad N_\varphi = \max(22, \lceil q_\varphi N_r \rceil^{1 \bmod 3}) \quad (36)$$

where q_ϑ and q_φ are parameters fixing the aspect ratio and the minimal values are not far from those found in the estimates above. The function $\lceil x \rceil^{a \bmod n}$ is the next number $x' \geq x$ ($x, x' \in \mathbb{N}$), for which $x' \equiv a \bmod n$.

4.6 Summary

The Yin-Yang grid allows an upgrade from the usual spherical polar coordinates to ones that avoid axial singularities and impose a less restrictive CFL-condition. At the same

time it, in principle, does not alter coordinates, but considers two mutually rotated patches. The price one pays are additional interpolations and transformations.

A bit of care is needed when comparing the grid resolutions of a code with usual spherical polar coordinates and of a Yin-Yang grid. Given $N_r \times N_\vartheta \times N_\varphi$ of the former, the nomenclature in case of a Yin-Yang grid would refer only to one patch and the number of grid cells would be, as a rule of thumb, $N_r \times N_\vartheta/2 \times 3N_\varphi/4$, with N_r, N_ϑ, N_φ being the grid cell numbers of a usual spherical polar coordinates code. The prescription may differ by some cells depending on the exact implementation. (See Eq. (35) for an example.)

For the cells to be equilateral on the equator in angular directions in a usual spherical polar coordinates code one has $N_\varphi = 2N_\vartheta$ because the domains of ϑ and φ differ by a factor of 2. In a Yin-Yang grid this factor is 3 and thus the choice of $N_\varphi = 3N_\vartheta$ is more appropriate. As the passage from one patch of the Yin-Yang grid to another approximately interchanges the roles of ϑ and φ, ϑ-φ-equilateral cells are in general considered to be favorable.

It seems that it would be desirable to find a grid setup without overlaps in order to avoid (non-conservative) interpolation. The challenge, however, is not to affect the implementation advantages of the Yin-Yang grid, e.g. the use of a convenient coordinate system, equivalent on both patches, and rectangular arrays. Under these constraints it seems virtually impossible to construct a non-overlapping grid. Clearly, the overlap in the original formulation comes from the fact, that the sphere has been dissected in two pieces by a line that is not invariant under the action of the rotation $\mathfrak{R}$. It is not hard to find such lines (think of a tennis ball). But they do not coincide with coordinate lines of ϑ or φ, and thus different coordinates must be invented. Once being ready to change for a different coordinate system, it is questionable why to stick to the concept of a Yin-Yang grid at all.

Additionally, even when there is no overlap between valid cells, due to the idea of finite differencing on stencils, ghost cells will have to fetch information from the other patch. If one wants to avoid interpolations the ghost cells would have to lie exactly at the same place as the valid cells of the other patch, thus putting severe conditions on the symmetry of coordinates near the edge of a patch. This problem appears for example in the cubed sphere-approach [RIP96], which can be viewed as a dissection of the sphere by an $\mathfrak{R}$-invariant curve (and subdividing each patch into three) and is the reason why (non-conservative) interpolations are still needed there as well.

5 Test cases

5.1 Quadrupole gravitational waves

As in Cartesian coordinates the travelling waves solution to the linearized Einstein equations is a superposition of plane waves, it can in polar coordinates be written down in a spherical harmonics expansion. The quadrupolar part of this expansion [Teu82] (see also [BMCCM13]) allows a test of spacetime evolution in a linearized problem with adjustable symmetry; it is moreover assumed to be the dominant part of the radiation. Testing spherical polar codes on axisymmetric waves probes not all of the implementation. On a Yin-Yang grid, however, the symmetry axis of the problem cannot coincide with the symmetry axis of the grid, as there are two of them. Even if the setup would be axisymmetric in one patch, it necessarily is not on the other. Thus, an axisymmetric quadrupole wave already suffices to test all of the code.

In Fig. 8 two numerical solutions are depicted together with the analytic solution. Fourth order finite differencing has been employed to approximate the derivatives. To suppress high frequency noise Kreiss-Oliger dissipation is used as in [BMCCM13] with the corresponding dimensionless coefficient set to $\eta = -0.005$.

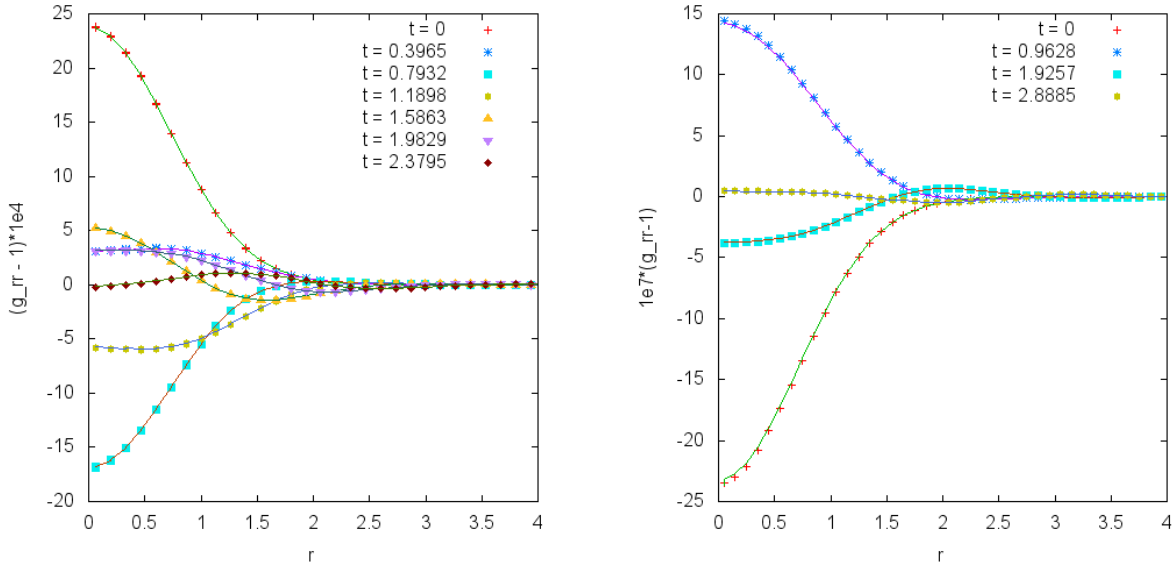

(a) (b)

Figure 8: For quadrupole waves of different symmetry m, the radial metric $\gamma_{rr} - 1$, normalised by the amplitude of the wave, is plotted as a function of radius at angular direction $(\vartheta, \varphi) = (\pi/2, \pi)$. (a): $m = 0$; (b): $m = 2$. The grid resolution is $30 \times 32 \times 97$ and $40 \times 16 \times 49$, respectively.

Choosing the wave amplitude small enough such that the linearized equations are valid

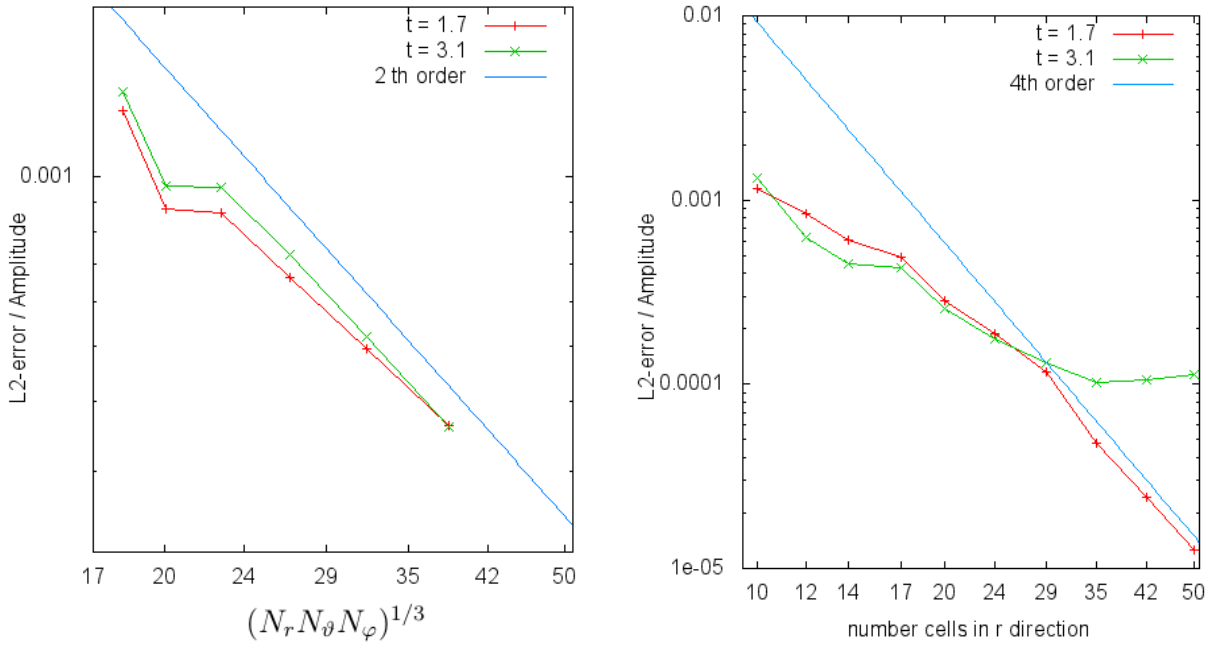

Figure 9: Convergence plots (double-logarithmic) for the $m = 2$ quadrupole waves showing the $\mathcal{L}_2$-norm of the error over the domain $r \in [0, 4]$ as a function of the number of cells in r-direction and at two different times. (a): 2^{nd} order interpolation between patches; (b): 4^{th} order interpolation between patches. The error stagnates at late times because the solution becomes affected by the outer boundary.

(10^{-7} is adapted), a convergence analysis can be performed (Fig. 9). Although only the number of cells in r-direction is given, the numbers in the other directions vary as well, in order to keep an approximately constant aspect ratio of the cells. Prescription (36) with $q_\vartheta = 0.4$ and $q_\varphi = 1.2$ was used. As this procedure yields slight deviations from a strictly linear increase, the error in Fig. 9a is plotted against $(N_r N_\vartheta N_\varphi)^{1/3}$.

The error is observed to stagnate at late times, because the solution becomes dominantly affected by influences from the outer boundary. In Fig. 10a the domain has been dissected into an inner ($r \leq \frac{r_{\max}}{3}$), an intermediate ($\frac{r_{\max}}{3} < r < \frac{2r_{\max}}{3}$), and an outer ($\frac{2r_{\max}}{3} < r < r_{\max}$) part, and the $\mathcal{L}_2$-error has been calculated separately for each of these parts. One observes that whereas the error roughly remains constant in the inner part, it quickly increases in the outer part and after $t \sim 2$ dominates the total one.

Finally, in Fig. 10b the runtimes for these tests are plotted together with the runtime of a usual spherical polar code on the same problem and machine (a desktop computer).

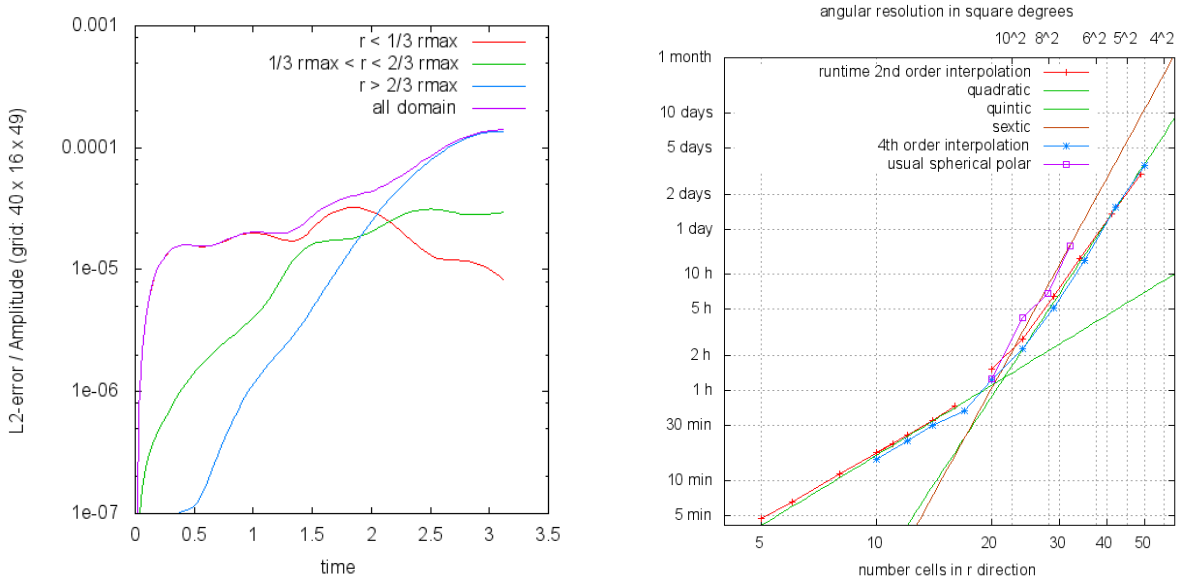

(a) (b)

Figure 10: (a) $\mathcal{L}_2$ norm of the error for a grid resolution $(40 \times 16 \times 49)$ as a function of time. The domain $r \in [0, 4]$ is dissected into three parts, and the error is integrated separately over them. At late times one observes an increase of the total error due to the outermost part of the domain. (b) Runtime of $m = 2$ quadrupole waves as a function of different grids. The number of cells in r-direction is given. For values less than 20 the number of cells in angular directions is constant (12×22), whereas for larger values they are augmented as before using $q_\vartheta = 0.4$ and $q_\varphi = 1.2$. Data are plotted for a Yin-Yang grid with 2^{nd} and 4^{th} order of interpolation between the patches, as well as for a usual spherical polar code with $(N_r \times N_\vartheta \times N_\varphi) = N_r(1 \times 0.8 \times 1.6)$ in order to have comparable cell dimensions. As expected from the definition of the CFL factor varying only the number of cells in r-direction yields a quadratically varying runtime, and keeping the aspect ratio of the cells constant – a quintic one. The influence of a higher order of interpolation is negligible. Usual spherical polar codes display a sextic runtime.

5.2 Relativistic shocks

Unidirectional shock tube tests and their spherically symmetric analogues can both be used to test the performance of relativistic hydrodynamics algorithms. The well-known classical analytic solution for the former has been extended to special relativity in [Tho86], and for arbitrary initial velocities in [MM94]. The spherically symmetric "explosions" can be compared to very well resolved solutions obtained with codes that solve the Einstein equations in spherical symmetry. The speed and height of the jumps can also be found analytically.

In the tests the domain $r \in [0, 10]$ is separated into two regions; the scalar hydrodynamic quantities differ from region to region but are initially constant inside each of them[9]. The fluid is initially at rest everywhere. The discontinuities then decay into the well-known structure of a rarefaction wave, a contact discontinuity and a shock. The spacetime is kept flat in these tests. They are all performed with the EOS of an ideal gas for an adiabatic constant of $\Gamma = 2$. For integrating the equations the HLLE solver ([HLL83], [Ein88]) with an MC limiter is used.

The first test presented has a high density region $r < 5$ with $(\rho_0, P) = (10, 13.33)$ and $(\rho_0, P) = (1, 0.66 \cdot 10^{-6})$ outside. In Fig. 11 and 12 two different codes have been run with this initial setup at high and low resolution. The solid lines show the initial setup and the results of a spherically symmetric code with $N_r = 600$. The non-constancy of the fluid state between shock and contact discontinuity and between contact discontinuity and rarefaction is due to the geometry of the problem and is observed in any kind of such "shock sphere" results. For scalar problems the shape of this curve can be calculated easily by the method of characteristics.

One observes furthermore that insufficient resolution smears the contact discontinuity significantly.

Centering now the high-density sphere not at $r = 0$ presents a stringent test for the performance of the hydrodynamic part of the equations on the Yin-Yang-grid with practically the same analytic solution. The high density region with the same values of the quantities is now a ball of radius 2 centered at $(r, \vartheta, \varphi) = (5, \pi/2, 0)$ (Fig. 13). For some time the two rarefaction waves do not interact and the solutions can be directly compared to those of the previous test. At late times the initially overdense region is completely emptied.

Another useful test is a unidirectional shock tube. If aligned with one of the coordinate axes in a Cartesian code, it would not test but a part of it; in a spherical polar code no derivatives or components vanish by symmetry. In a Yin-Yang-code additionally the quality of communication between patches can be studied. This test has already been used for non-relativistic hydrodynamics on a Yin-Yang grid in [WHM10]. There however a ball around the origin was excluded from the computational domain. The setup adapted here is $(\rho_0, P) = (0.2, 0.1)$ for $x = r \cos\varphi \sin\vartheta > 5$ and $(\rho_0, P) = (0.1, 0.03)$ everywhere else on a domain $r \in [0, 10]$. Initially the fluid is at rest (Fig. 15).

[9] To visualize the setup small icons next to the plots depict the equatorial plane and the low and high density regions. A red line shows the orientation of the plot.

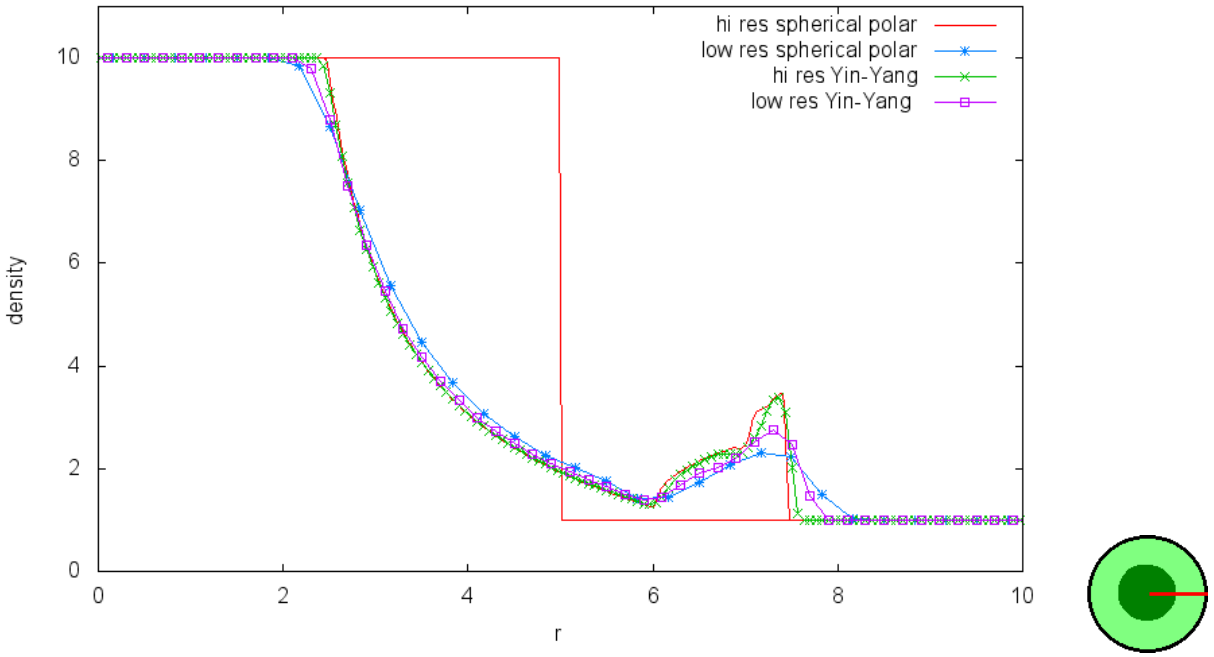

Figure 11: Density over radius in the direction $(\vartheta, \varphi) = (\pi/2, 0)$ at $t = 3$. Solid red line: Initial data and solution obtained with a spherically symmetric code resolving the domain $r \in [0, 10]$ with 600 points. Green crosses: solution obtained with a Yin-Yang grid of $150 \times 12 \times 22$ cells. Blue crosses and violet boxes: low resolution runs with usual spherical polar coordinates ($N_r = 30$), and the Yin-Yang grid $(50 \times 12 \times 22)$, respectively. For the icon, see Footnote 9.

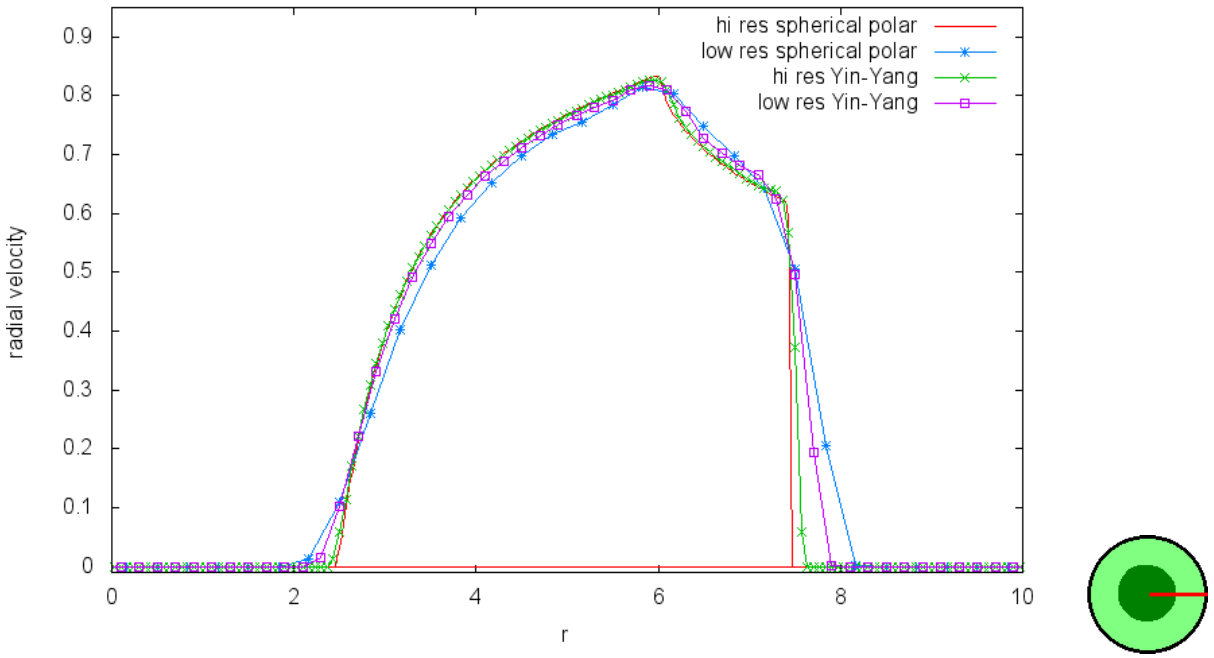

Figure 12: Same as Fig. 11, but plotting the radial velocity.

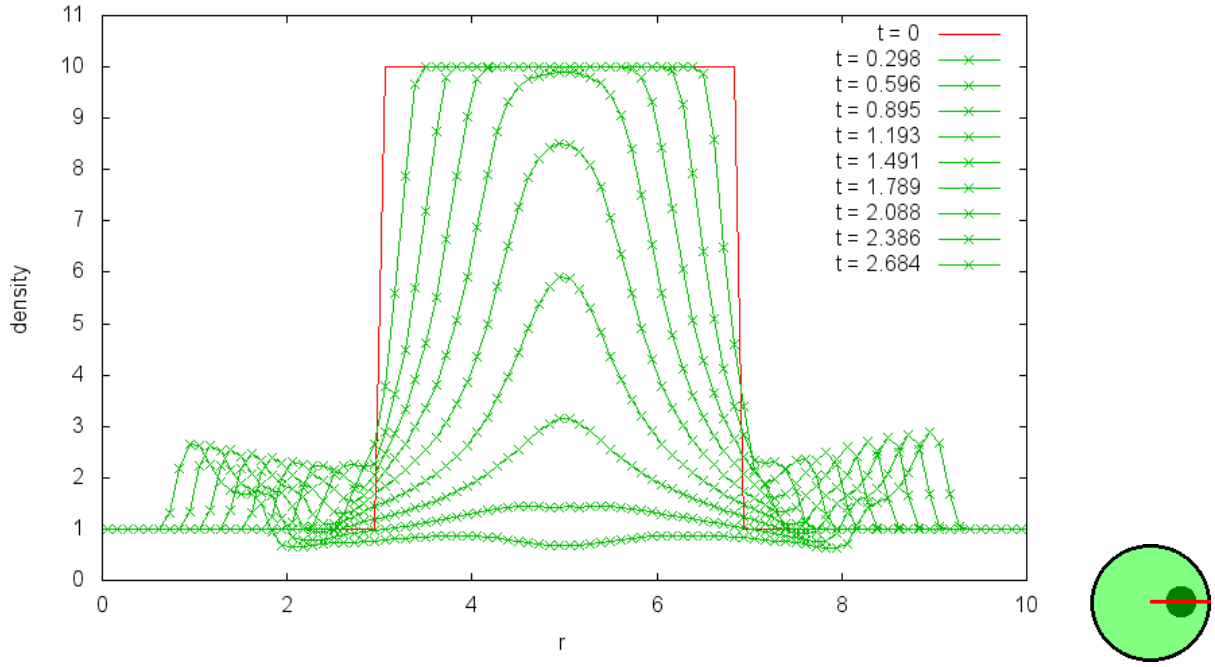

Figure 13: Density over radius in the direction $(\vartheta, \varphi) = (\pi/2, 0)$. Solid red line: Initial data. In green the solution for different times obtained with a Yin-Yang grid $(90 \times 20 \times 61)$. The slight differences in the resolution of the contact discontinuity have to be considered minding that the r-φ-aspect ratio of the respective cells differs by a factor of ~ 9. For the icon, see Footnote 9.

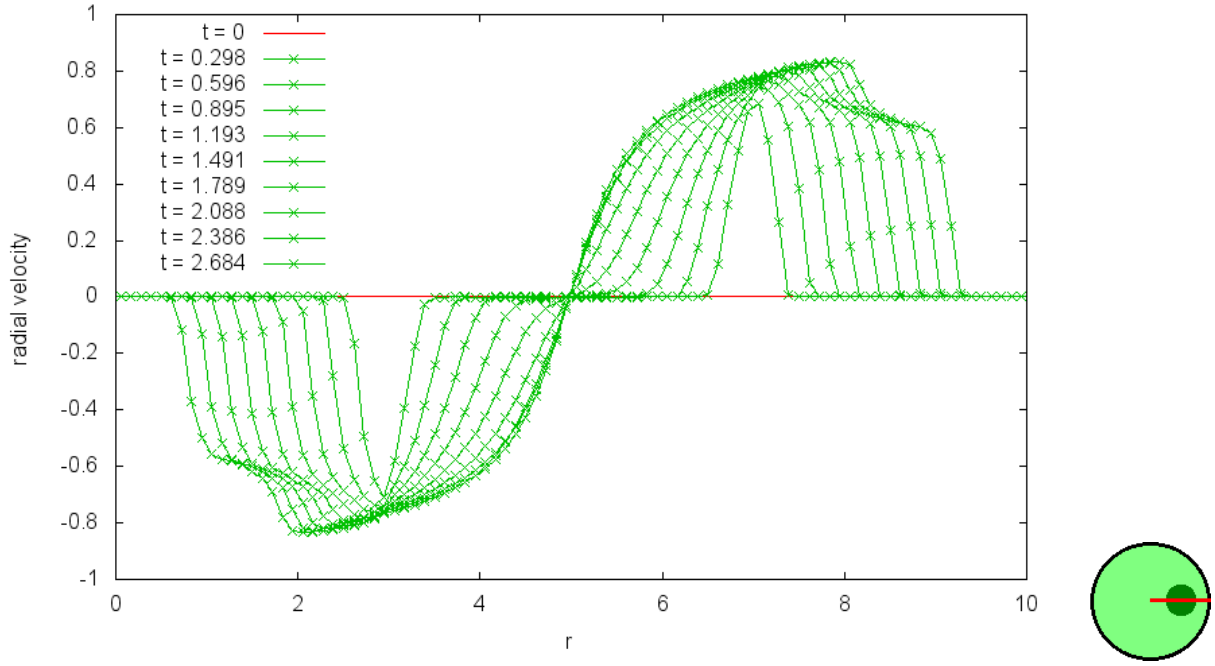

Figure 14: Same as Fig. 13, but plotting the radial velocity.

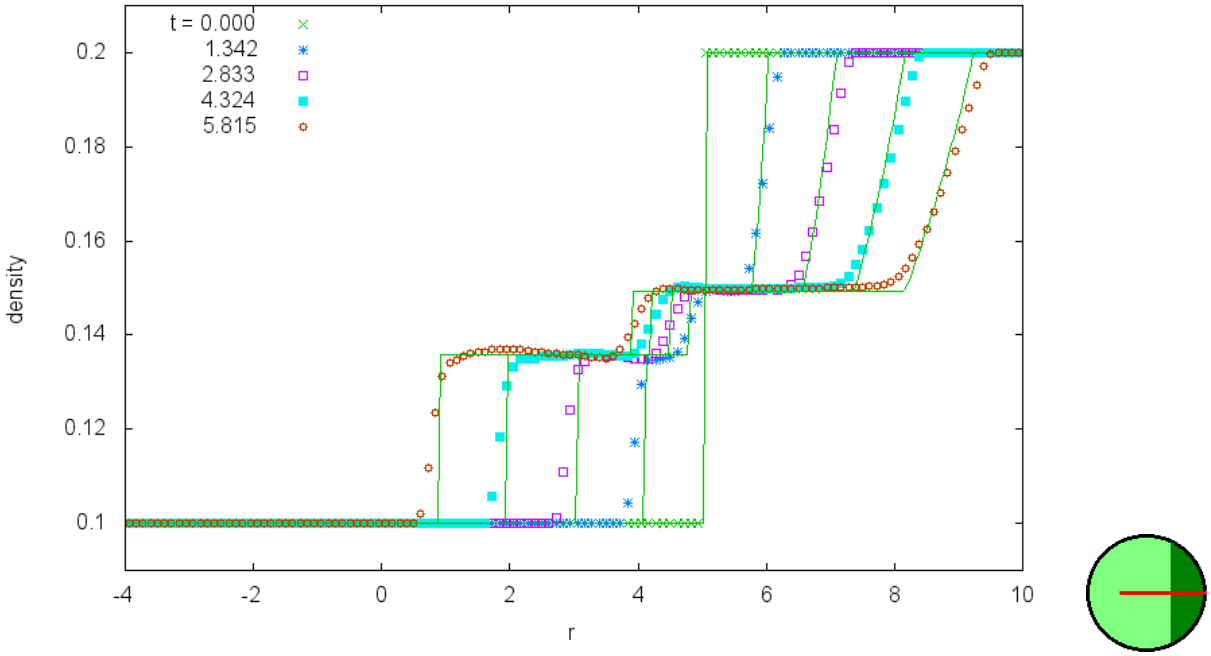

Figure 15: Density over radius in the direction $(\vartheta, \varphi) = (\pi/2, 0)$ on a Yin-Yang grid $(90 \times 20 \times 61)$ at different times. Solid lines show the analytic solution. For the icon, see Footnote 9.

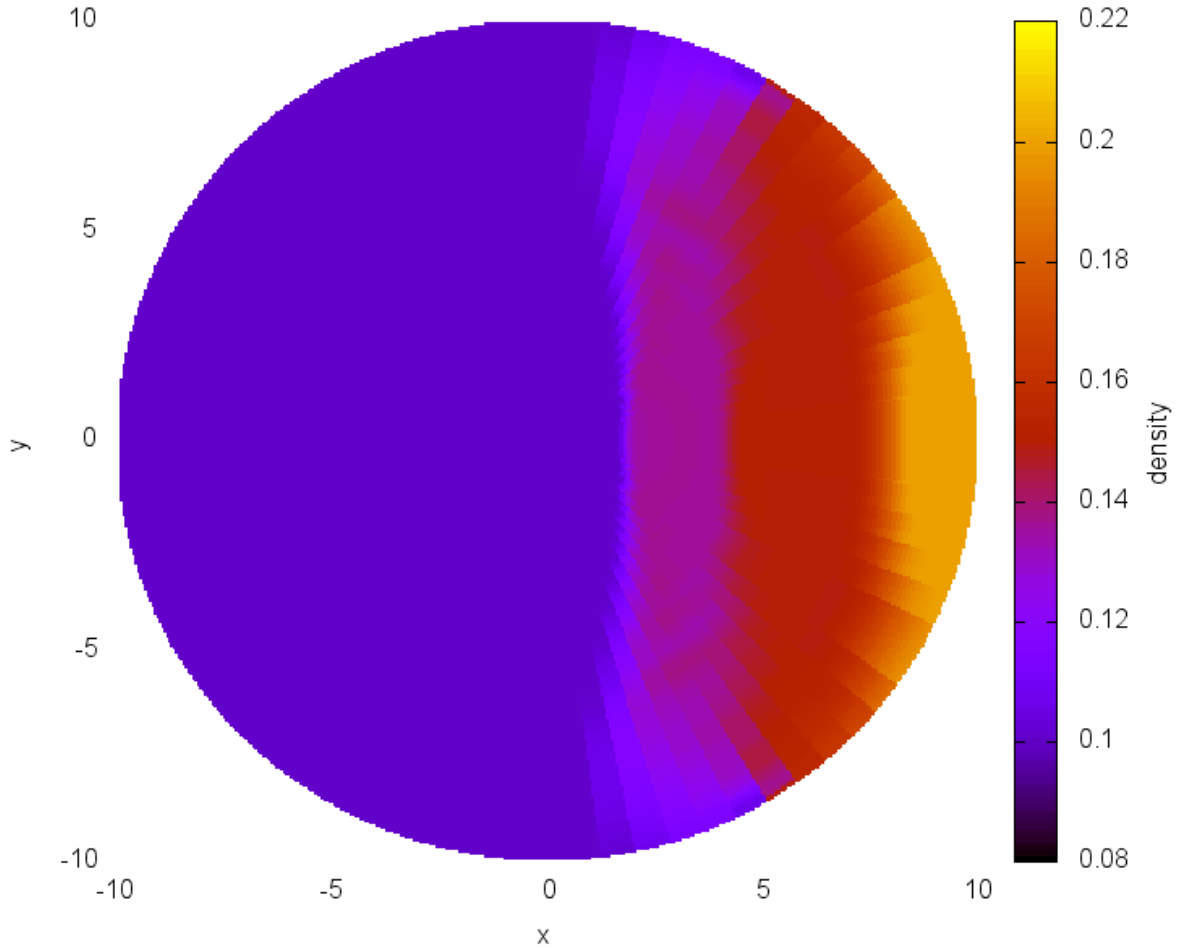

Figure 16: Same setup as Fig. 15, at time $t = 4.324$. The image shows the density (colour-coded) on the equatorial plane. The boundary between the two grids is at $x = \pm y$ for positive x (i.e. at $\varphi = \pm\pi/4$). A slight difference in the angular resolution can be observed between the two patches, but is due to resampling, when data from both grids are interpolated onto the equatorial plane. The shocks remain straight even after having passed through the boundary between the patches. The shock front distortions near the outer boundary are due to outflow boundary conditions.

6 Summary and outlook

Chandrasekhar quotes Max Born in [Cha84] as having written

> *It [the general theory of relativity] appeared to me like a great work of art, to be enjoyed and admired from a distance.*

It is indeed an amazing theory, combining so much of deep mathematics with such complicated answers to such fundamental questions. It is also in many aspects an outstanding theory, having been found on theoretical grounds and not by inspection of experimental data. It also appeared just a decade before quantum theory showed its deficiency, although up to present times it is unclear how a reconciliation would look like and at what energy scales to expect its effects to show up.

General relativity predictions have been so far consistently verified, as far as experimental methods were available. This concerns tests in the solar system (including relativistic corrections to routine satellite operation), gravitational lensing, pulsar timing and many others. At the same time a lot more tests of general relativity at large scales and in strong fields are desirable; the first direct detection of gravitational waves is therefore expected to open up a new field in astronomy.

Solutions to the Einstein equations turn out to be hard to obtain. Analytic approximation techniques have provided valuable results, but cannot be used to obtain solutions that describe compact astrophysical objects, such as neutron stars and black holes, adequately. Stationary analytic solutions (Schwarzschild, Kerr) have given valuable insight, but models of spacetime with matter that shall be compared to observations have so far to be computed numerically. This goes in parallel with the steady increase of available computational power.

Numerical relativity is a diverse field with a large number of proposed approaches, that has been steadily learning how to handle its challenges over the last decades. Numerical relativity on spherical polar and multipatch grids can be seen as one further step in the exploration of the numerical behaviour of the equations.

This thesis presented an implementation of the Yin-Yang grid for general relativistic hydrodynamics and spacetime evolution in the BSSN formulation. A patch of spherical polar coordinates next to the equator is used twice to cover every 2-sphere in a singularity-free manner. The two patches have together an overlap of at least $\sim 6\%$ of the surface area of the sphere. Starting with a code in spherical polar coordinates, the numerical algorithms have to be augmented by a communication procedure between the two patches and have to take care of the correct transformations when setting up initial data or producing outputs. In order to be able to evaluate the finite differencing formulae that replace derivatives, cells near the boundary of one patch have to look up the corresponding values on the other patch. For non-scalar quantities this means also transforming them from the other patch's coordinate system. The Yin-Yang grid is in this respect a very symmetric setup, and by virtue of its use of standard spherical polar coordinates (albeit

twice) a particularly attractive one. It eliminates the coordinate singularities on the polar axis which accumulate numerical errors due to diverging terms and impose a restrictive Courant condition due to converging coordinate lines. The time step of the Yin-Yang grid is dominated by the converging coordinate lines in the vicinity of the origin $r = 0$, which is unaffected by the Yin-Yang approach. Therefore it easily achieves an order of magnitude speedup, despite redundant calculations in the overlap region and additional interpolations and transformations, which however happen at either only a fraction of the cells (patch boundaries) or a fraction of the computational time (initial data, outputs).

This grid has been so far found to perform well and stably with both vacuum and non-vacuum spacetimes. As mathematical statements about the convergence of a given method are very rare, further work is needed to evaluate the performance of the grid in a large variety of situations. This includes studies of both analytically known and astrophysically relevant solutions as well as further investigation of their properties in the given formulation of the equations, especially with respect to the coordinate evolution.

Another direction of investigation are more flexible grid geometries, adapted to the problem at hand, schemes of higher accuracy and needing less computational time. As inspiration, numerical hydrodynamics offers a variety of ideas in all these aspects, but surely numerical relativity will in future also offer new, innovative solutions in this respect.

7 Appendix

7.1 On global hyperbolicity

Details on the definitions and theorems of this section can be found in [O'N83], [Gal14] and [Rin09]. The timelike and causal future of $p \in M$ is denoted by $I^+(p)$ and $J^+(p)$, respectively, i.e.

$$I^+(p) = \{q \in M : q \text{ can be connected to } p \text{ by a future directed timelike curve in } M\}$$
$$J^+(p) = \{q \in M : q \text{ can be connected to } p \text{ by a future directed causal curve in } M\} \cup \{p\}$$

Analogous definitions can be given for the pasts, denoted by I^- and J^-.

An open set U in spacetime M is said to be *causally convex* provided no causal curve in M meets U in a disconnected set. A spacetime M is called *strongly causal* if any of its points has arbitrarily small causally convex neighbourhoods. This definition is a stronger version of just a *causal* spacetime, which does not contain closed causal curves, as it turns out that such a spacetime would still allow curves that are as near as one wishes to being closed.

A spacetime M is called *globally hyperbolic* if it is strongly causal and the sets $J^+(p) \cap J^-(q)$ are compact for all $p, q \in M$. The latter property is referred to as *internal compactness*. Geroch [Ger70] proved that if a spacetime admits a Cauchy surface it is globally hyperbolic, and conversely. In the proof he constructed a C^0 *time function*, i.e. a function that is strictly increasing along future directed causal curves. By considering level sets this function is used to show that a globally hyperbolic spacetime with a Cauchy surface Σ is necessarily homeomorphic to $\Sigma \times I$ (with I an interval, that can, if needed, be rescaled to $\mathbb{R}$).

As has been proven by Choquet-Bruhat [FB52] that, given vacuum initial data (Σ, g, K), i.e. covariant 2-tensors g and K on a 3-dimensional manifold Σ, there exists a solution $(M, {}^4g)$ to the Einstein vacuum equations and an embedding $i : \Sigma \to M$ such that

$$i^*g = {}^4g \quad g \text{ becomes the metric on } i(\Sigma)$$
$$i^*K = {}^4K \quad K \text{ becomes the exterior curvature on } i(\Sigma)$$

and $i(\Sigma)$ is a Cauchy hypersurface in $(M, {}^4g)$.
$(M, {}^4g)$ is called a *globally hyperbolic development*.

Speaking losely, when starting out from a Cauchy surface as initial data, one obtains a globally hyperbolic spacetime that fullfills the Einstein equations and gives naturally a slicing. The converse is a bit more subtle:

A spacetime M is said to be *regularly sliced* if $M = \Sigma \times I$ with Σ a Cauchy surface and I an interval of $\mathbb{R}$ (possibly infinite), the spacetime metric ${}^4g$ can be written as

${}^4g = -\alpha^2(\mathrm{d}x^0)^2 + g_{ij}\mathrm{d}x^i \otimes \mathrm{d}x^j$ with the α bounded from below and from above by positive numbers, the spacelike slices are Riemannian manifolds with t-dependent metrics uniformly bounded below, as well as the norm of the vector β uniformly bounded [CB08].

Now by [CBC02] a regularly sliced spacetime is globally hyperbolic.

Citing for the mathematically interested reader further from [CB08] (p. 422): "It results from the definition of global hyperbolicity that a nakedly singular spacetime is not globally hyperbolic. Penrose proves that, conversely if a space is strongly causal and is not nakedly singular it is globally hyperbolic. This led to the strong cosmic censorship conjecture, saying in a rather loose way that all "reasonable" Einsteinian spacetimes ought to be globally hyperbolic, in particular they should never be nakedly singular". However the precise formulations of the corresponding conjectures, to say nothing of their eventual confirmations, are still under debate.

7.2 Test of tensor transformations

If a matrix has to be specified as it will be after transformation, one writes down

$$\begin{aligned}\tilde{g} = \mathfrak{M}g\mathfrak{M}^{-1} &= \begin{pmatrix} D & -F \\ F & D \end{pmatrix}\begin{pmatrix} \alpha & \beta \\ \beta & \gamma \end{pmatrix}\begin{pmatrix} D & F \\ -F & D \end{pmatrix} \\ &= \begin{pmatrix} \alpha D^2 + \gamma F^2 - 2\beta FD & FD(\alpha-\gamma) + \beta(D^2-F^2) \\ FD(\alpha-\gamma) + \beta(D^2-F^2) & \alpha F^2 + \gamma D^2 + 2\beta FD \end{pmatrix} \stackrel{!}{=} \begin{pmatrix} x & p \\ p & y \end{pmatrix}\end{aligned}$$

with $D = -\sin\varphi\sin\tilde{\varphi}$ and $F = \cos\varphi/\sin\tilde{\vartheta}$ and where α, β, γ are to be determined as functions of x, y, p. As solution one finds

$$\begin{aligned}\alpha &= F^2(x+y) + 2FDp + (D^2-F^2)x \\ \beta &= FD(x+y) - 2FDx + (D^2-F^2)p \\ \alpha + \gamma &= x + y\end{aligned}$$

using $F^2 + D^2 = 1$.

References

[ABD+03] Miguel Alcubierre, Bernd Brügmann, Peter Diener, Michael Koppitz, Denis Pollney, Edward Seidel, and Ryoji Takahashi. Gauge conditions for long-term numerical black hole evolutions without excision. *Physical Review D*, 67(8):084023, 2003.

[ADM08] Richard Arnowitt, Stanley Deser, and Charles W Misner. Republication of: The dynamics of general relativity. *General Relativity and Gravitation*, 40(9):1997–2027, 1962, republ. 2008.

[Alc97] Miguel Alcubierre. Appearance of coordinate shocks in hyperbolic formalisms of general relativity. *Physical Review D*, 55(10):5981, 1997.

[BAF84] Matania Ben-Artzi and Joseph Falcovitz. A second-order godunov-type scheme for compressible fluid dynamics. *Journal of Computational Physics*, 55(1):1–32, 1984.

[BGGN04] Silvano Bonazzola, Eric Gourgoulhon, Philippe Grandclement, and Jerome Novak. Constrained scheme for the einstein equations based on the dirac gauge and spherical coordinates. *Physical Review D*, 70(10):104007, 2004.

[BLPŽ03] C Bona, T Ledvinka, C Palenzuela, and M Žáček. General-covariant evolution formalism for numerical relativity. *Physical Review D*, 67(10):104005, 2003.

[BMCCM13] Thomas W Baumgarte, Pedro J Montero, Isabel Cordero-Carrión, and Ewald Müller. Numerical relativity in spherical polar coordinates: Evolution calculations with the bssn formulation. *Physical Review D*, 87(4):044026, 2013.

[BMSS95] Carles Bona, Joan Masso, Edward Seidel, and Joan Stela. New formalism for numerical relativity. *Physical Review Letters*, 75(4):600, 1995.

[BPL05] Carles Bona and Carlos Palenzuela-Luque. *Elements of Numerical Relativity: From Einstein's Equations to Black Hole Simulations*. Springer, 2005.

[Bro09] J David Brown. Covariant formulations of baumgarte, shapiro, shibata, and nakamura and the standard gauge. *Physical Review D*, 79(10):104029, 2009.

[BS98] Thomas W Baumgarte and Stuart L Shapiro. Numerical integration of einsteins field equations. *Physical Review D*, 59(2):024007, 1998.

[CB08] Yvonne Choquet-Bruhat. *General relativity and the Einstein equations*. Oxford University Press, 2008.

[CBC02] Yvonne Choquet-Bruhat and Spiros Cotsakis. Global hyperbolicity and completeness. *Journal of Geometry and Physics*, 43(4):345–350, 2002.

[CCCD12] Isabel Cordero-Carrión and Pablo Cerdá-Durán. Partially implicit runge-kutta methods for wave-like equations in spherical-type coordinates. *arXiv preprint arXiv:1211.5930*, 2012.

[CDH+08] Phillip Colella, Milo R Dorr, Jeffrey AF Hittinger, P McCorquodale, and Daniel F Martin. High-order, finite-volume methods on locally-structured grids. *Numerical Modeling of Space Plasma Flows: Astronum*, 406:207–216, 2008.

[CFL28] Richard Courant, Kurt Friedrichs, and Hans Lewy. Über die partiellen differenzengleichungen der mathematischen physik. *Mathematische Annalen*, 100(1):32–74, 1928.

[Cha84] S Chandrasekhar. The general theory of relativity- why'it is probably the most beautiful of all existing theories'. *Journal of Astrophysics and Astronomy*, 5:3–11, 1984.

[CS98] Bernardo Cockburn and Chi-Wang Shu. The runge–kutta discontinuous galerkin method for conservation laws v: multidimensional systems. *Journal of Computational Physics*, 141(2):199–224, 1998.

[CW84] Phillip Colella and Paul R Woodward. The piecewise parabolic method (ppm) for gas-dynamical simulations. *Journal of computational physics*, 54(1):174–201, 1984.

[DET07] Michael Dumbser, C Enaux, and E Toro. Explicit finite volume schemes of arbitrary high order of accuracy for hyperbolic systems with stiff source terms. *J. Comput. Phys*, pages 1049–1063, 2007.

[Ein88] Bernd Einfeldt. On godunov-type methods for gas dynamics. *SIAM Journal on Numerical Analysis*, 25(2):294–318, 1988.

[FB52] Yvonne Foures-Bruhat. Théorème d'existence pour certains systèmes d'équations aux dérivées partielles non linéaires. *Acta mathematica*, 88(1):141–225, 1952.

[Fri97] Simonetta Frittelli. Note on the propagation of the constraints in standard 3+ 1 general relativity. *Physical Review D*, 55(10):5992, 1997.

[Gal14] Gregory J Galloway. Notes on lorentzian causality. ESI-EMS-IAMP Summer School, `http://www.math.miami.edu/~galloway/vienna-course-notes.pdf`, 2014.

[Gau28] Carl Friedrich Gauss. *Disquisitiones generales circa superficies curvas*. Typis Dieterichianis, 1828.

[Ger70] Robert Geroch. Domain of dependence. *Journal of Mathematical Physics*, 11(2):437–449, 1970.

[God59] Sergei Konstantinovich Godunov. A difference method for numerical calculation of discontinuous solutions of the equations of hydrodynamics. *Matematicheskii Sbornik*, 89(3):271–306, 1959.

[Gou12] Eric Gourgoulhon. *3+ 1 formalism in general relativity: bases of numerical relativity*, volume 846. Springer, 2012.

[GR62] W Lawrence Gates and Christopher A Riegel. A study of numerical errors in the integration of barotropic flow on a spherical grid. *Journal of geophysical research*, 67(2):773–784, 1962.

[GS98] Sigal Gottlieb and Chi-Wang Shu. Total variation diminishing runge-kutta schemes. *Mathematics of Computation of the American Mathematical Society*, 67(221):73–85, 1998.

[GSKM14] Hannes Grimm-Strele, Friedrich Kupka, and Herbert J Muthsam. Curvilinear grids for weno methods in astrophysical simulations. *Computer Physics Communications*, 185(3):764–776, 2014.

[Har83] Ami Harten. High resolution schemes for hyperbolic conservation laws. *Journal of computational physics*, 49(3):357–393, 1983.

[HEOC87] Ami Harten, Bjorn Engquist, Stanley Osher, and Sukumar R Chakravarthy. Uniformly high order accurate essentially non-oscillatory schemes, iii. *Journal of computational physics*, 71(2):231–303, 1987.

[Hir68] CW Hirt. Heuristic stability theory for finite-difference equations. *Journal of Computational Physics*, 2(4):339–355, 1968.

[HLL83] Amiram Harten, Peter D Lax, and Bram van Leer. On upstream differencing and godunov-type schemes for hyperbolic conservation laws. *SIAM review*, 25(1):35–61, 1983.

[Ise07] James A Isenberg. Waveless approximation theories of gravity. *arXiv preprint gr-qc/0702113*, 1978,2007.

[Kol11] V.P. Kolgan. Application of the principle of minimizing the derivative to the construction of finite-difference schemes for computing discontinuous solutions of gas dynamics. *Journal of Computational Physics*, 230(7):2384 – 2390, 1972/transl. 2011.

[KS04] Akira Kageyama and Tetsuya Sato. yin-yang grid: An overset grid in spherical geometry. *Geochemistry, Geophysics, Geosystems*, 5(9), 2004.

[LeV02] Randall J LeVeque. *Finite volume methods for hyperbolic problems*, volume 31. Cambridge university press, 2002.

[Lic44] A. Lichnerowicz. L'integration des équations de la gravitation relativiste et le problème des n corps. *J. Math. Pures Appl.*, 23:37–63, 1944.

[LOC94] Xu-Dong Liu, Stanley Osher, and Tony Chan. Weighted essentially non-oscillatory schemes. *Journal of computational physics*, 115(1):200–212, 1994.

[LW60] Peter Lax and Burton Wendroff. Systems of conservation laws. *Communications on Pure and Applied mathematics*, 13(2):217–237, 1960.

[MBM14] Pedro J Montero, Thomas W Baumgarte, and Ewald Müller. General relativistic hydrodynamics in curvilinear coordinates. *Physical Review D*, 89(8):084043, 2014.

[MM94] José Ma Martí and Ewald Müller. The analytical solution of the riemann problem in relativistic hydrodynamics. *Journal of Fluid Mechanics*, 258:317–333, 1994.

[O'N83] Barrett O'Neill. *Semi-Riemannian Geometry With Applications to Relativity, 103*, volume 103. Academic press, 1983.

[Phi59] Norman A Phillips. *Numerical integration of the primitive equations on the hemisphere*. Massachusetts Institute of Technology, 1959.

[Pre05] Frans Pretorius. Numerical relativity using a generalized harmonic decomposition. *Classical and Quantum Gravity*, 22(2):425, 2005.

[PXT06] Xindong Peng, Feng Xiao, and Keiko Takahashi. Conservative constraint for a quasi-uniform overset grid on the sphere. *Quarterly Journal of the Royal Meteorological Society*, 132(616):979–996, 2006.

[Rin09] Hans Ringström. *The Cauchy problem in general relativity*. European Mathematical Society, 2009.

[RIP96] C Ronchi, R Iacono, and Pier S Paolucci. The cubed sphere: a new method for the solution of partial differential equations in spherical geometry. *Journal of Computational Physics*, 124(1):93–114, 1996.

[Roe81] Philip L Roe. Approximate riemann solvers, parameter vectors, and difference schemes. *Journal of computational physics*, 43(2):357–372, 1981.

[RRH+02] David A Randall, Todd D Ringler, Ross P Heikes, Phil Jones, and John Baumgardner. Climate modeling with spherical geodesic grids. *Computing in Science and Engineering*, 4(5):32–41, 2002.

[Sad72] Robert Sadourny. Conservative finite-difference approximations of the primitive equations on quasi-uniform spherical grids. *Monthly Weather Review*, 100(2):136–144, 1972.

[SAM68] Robert Sadourny, Akio Arakawa, and Yale Mintz. Integration of the nondivergent barotropic vorticity equation with an icosahedral-hexagonal grid for the sphere 1. *Monthly Weather Review*, 96(6):351–356, 1968.

[Smo83] Joel Smoller. Shock waves and reaction-diffusion equations. In *Springer-Verlag (Grundlehren der Mathematischen Wissenschaften. Volume 258), 1983, 600 p.*, volume 258, 1983.

[SN95] Masaru Shibata and Takashi Nakamura. Evolution of three-dimensional gravitational waves: Harmonic slicing case. *Physical Review D*, 52(10):5428, 1995.

[SO88] Chi-Wang Shu and Stanley Osher. Efficient implementation of essentially non-oscillatory shock-capturing schemes. *Journal of Computational Physics*, 77(2):439–471, 1988.

[Teu82] Saul A Teukolsky. Linearized quadrupole waves in general relativity and the motion of test particles. *Physical Review D*, 26(4):745, 1982.

[Tho86] Kevin W Thompson. The special relativistic shock tube. *Journal of Fluid Mechanics*, 171:365–375, 1986.

[TMN01] EF Toro, RC Millington, and LAM Nejad. Towards very high order godunov schemes. In *Godunov Methods*, pages 907–940. Springer, 2001.

[vL73] Bram van Leer. Towards the ultimate conservative difference scheme i. the quest of monotonicity. In *Proceedings of the Third International Conference on Numerical Methods in Fluid Mechanics*, pages 163–168. Springer, 1973.

[vL79] Bram van Leer. Towards the ultimate conservative difference scheme. v. a second-order sequel to godunov's method. *Journal of computational Physics*, 32(1):101–136, 1979.

[vL06] Bram van Leer. Upwind and high-resolution methods for compressible flow: From donor cell to residual-distribution schemes. *Communications in Computational Physics*, 1(192-206):12, 2006.

[WHM10] Annop Wongwathanarat, Nicolay J Hammer, and Ewald Müller. An axis-free overset grid in spherical polar coordinates for simulating 3d self-gravitating flows. *arXiv preprint arXiv:1003.1633*, 2010.

[Wil68] David L Williamson. Integration of the barotropic vorticity equation on a spherical geodesic grid. *Tellus*, 20(4):642–653, 1968.

[Win05] J Winicour. Characteristic evolution and matching living rev. *Relativity*, 8(10), 2005.

[WMM96] JR Wilson, GJ Mathews, and P Marronetti. Relativistic numerical model for close neutron-star binaries. *Physical Review D*, 54(2):1317, 1996.

[YJ71] James W York Jr. Gravitational degrees of freedom and the initial-value problem. *Physical Review Letters*, 26(26):1656, 1971.

[YJ04] James W York Jr. Velocities and momenta in an extended elliptic form of the initial value conditions. *arXiv preprint gr-qc/0409102*, 2004.

Erklärung

Ich versichere, diese Arbeit selbstständig verfasst und keine anderen als die angegebenen Quellen und Hilfsmittel benutzt zu haben.

Heidelberg, den